# A Framework for Parameter Estimation, Sensitivity Analysis, and Uncertainty Analysis for Holistic Hydrologic Modeling Using SWAT+

Salam A. Abbas[1], Ryan T. Bailey[1], Jeremy T. White[2], Jeffrey G. Arnold[3], Michael J. White[3], Natalja Cerkasova[4], Jungang Gao[4]

[1] Department of Civil and Environmental Engineering, Colorado State University, USA.
[2] INTERA, Inc. Perth Australia.
[3] Grassland Soil and Water Research Laboratory, USDA–ARS, Temple, TX, 76502, USA.
[4] Blackland Research & Extension Center, Texas A&M AgriLife, Temple, TX, 76502, USA.

*Correspondence to*: Salam A. Abbas (salam.a.abbas@colostate.edu)

**Abstract.** Parameter Sensitivity analysis plays a critical role in efficiently determining main parameters, enhancing the effectiveness of estimation of parameters, and uncertainty quantification in hydrologic modeling. In this paper, we demonstrate uncertainty and sensitivity analysis technique for the holistic Soil and Water Assessment Tool (SWAT+) model, coupled with new *gwflow* module, spatially distributed, physically based groundwater flow modeling. Main calculated groundwater inflows and outflows include boundary exchange, pumping, saturation excess flow, groundwater-surface water exchange, recharge, groundwater-lake exchange, and tile drainage outflow. We present the method for four watersheds located in different areas of the United States for 16 years (2000–2015), emphasizing regions of extensive tile drainage (Winnebago River, Minnesota, Iowa), intensive surface-groundwater interaction (Nanticoke River, Delaware, Maryland), groundwater pumping for irrigation (Cache River, Missouri, Arkansas), and mountain snowmelt (Arkansas Headwaters, Colorado).

The main parameters of coupled SWAT+*gwflow* model are estimated utilizing the parameter estimation software (PEST). The monthly streamflow of holistic SWAT+*gwflow* is evaluated based Nash-Sutcliffe efficiency index (NSE), percentage bias (PBIAS), determination coefficient ($R^2$), and Kling-Gupta efficiency coefficient (KGE), whereas groundwater head is evaluated using mean absolute error (MAE). The Morris method is employed to identify the key parameters influencing hydrological fluxes. Furthermore, the iterative ensemble smoother (iES) is utilized as a technique for Uncertainty Quantification (UQ) and Parameter Estimation (PE) and to decrease the computational cost owing to the large number of parameters.

Depending on the watershed, key identified selected parameters include aquifer specific yield, aquifer hydraulic conductivity, recharge delay, streambed thickness, streambed hydraulic conductivity, area of groundwater inflow to tile, depth of tiles below ground surface, hydraulic conductivity of the drain perimeter, river depth (for groundwater flow processes); runoff curve number (for surface runoff processes); plant uptake compensation factor, soil evaporation compensation factor (for Potential and actual evapotranspiration processes); soil available water capacity, percolation

coefficient (for Soil water processes). The presence of *gwflow* parameters permits for the recognition of all key parameters in the surface/subsurface flow processes, with results substantially differing if the base SWAT+ models are utilized.

**Keywords:**

model calibration; SWAT+; *gwflow*; parameter sensitivity; Morris screening; uncertainty quantification; iterative ensemble smoothers.

## 1 Introduction

Hydrologic models have been developed to enhance understanding of the dynamics of hydrological fluxes to address practical issues related to water resources management (Liu et al., 2020; Wei et al., 2018), especially under the influence of anthropogenic activities and climate change, which can result in significant changes in the hydrological system (Abbas et al., 2022; Pokhrel et al., 2021). Typically, hydrologic models include several parameters to represent the hydrologic processes and to consider spatial variations resulting from climate, soil type, land use, etc. (Fatichi et al., 2016; Čerkasova et al., 2021). To employ hydrologic models in a responsible manner for system understanding and scenario analysis, sensitivity analysis (SA), uncertainty analysis (UA), and parameter estimation (PE) are key steps in the modeling process due to the presence of spatial heterogeneities (Bennett et al., 2013; Doherty and Hunt, 2009) and often the use of a broad suite of model parameters. SA identifies model parameters that have a strong influence on model output (e.g., streamflow), and results generally can provide insights into system behavior and point to system parameters that require more data collection or management strategies that may be efficient in controlling a certain system response (Leta et al., 2015). UA relates uncertainty in model parameters to model output, and hence can provide ranges of system output possibilities, e.g., when using the model in scenario analysis as a decision support tool, to answer questions regarding effects of system changes. PE provides the best values for matching model predictions to historical observations.

SA methods can be classified into local sensitivity analysis (LSA) and global sensitivity analysis (GSA) (Santos et al., 2022). Examples of LSA approaches are one–variable–at–a–time (OAT) and the differential analysis (DA) method (Devak and Dhanya, 2017), are less reputable since they disregard to consider the interaction between several parameters and cannot precisely estimate optimal parameters value (Helton, 1993). While GSA techniques such as regional sensitivity analysis (RSA), Morris screening, variance-based sensitivity analysis (Sobol's method), and Fourier amplitude sensitivity test (FAST), have been developed and used in many applications (Olaya–Abril et al., 2017; Devak and Dhanya, 2017). These methods take into account the interaction between different parameters by altering several parameters of model together (Pianosi et al., 2017; Devak and Dhanya, 2017). GSA is gaining prominence in hydrologic and environmental modeling (e.g., Plischke et al., 2013; Pianosi et al., 2017). GSA is employed for the detection of insignificant parameters and the identification of influential parameters with a significant impact on model outputs (Santos et al., 2022).

Other GSA applications include identification of model behavior, prioritization for uncertainty estimation and reduction, and for simplification of the model (Pianosi et al., 2017). However, these methods typically require a large number of model evaluations. More recently, iterative ensemble smoother (iES) techniques have been developed for uncertainty quantification (UQ) and for more efficient parameter estimations (PE) by reducing the number of model evaluations incurred by large number of parameters (Chen and Oliver, 2012); this technique can be implemented in a non-intrusive/model-independent approach, resulting in a desirable option for application to analyses of hydrologic and environmental modeling. The iES has been utilized in several applications (e.g., Bocquet and Sakov, 2014; Crestani et al., 2013).

Null-Space Monte Carlo approach (NSMC) is not dissimilar to the iES approach in their goals: to represent posterior parameter uncertainty, especially as it relates to null-space parameters and parameter components (i.e., nonunique parameters). However, NSMC uses a full rank Jacobian filled using finite difference perturbations, linearized at the final calibration parameter set to project a prior parameter ensemble, realization by realization, toward being "calibrated" under the assumption of linearity. In contrast, the iES approach propagates the prior parameter ensemble directly during history matching and avoids filling a full-rank Jacobian, and instead uses an ensemble-approximation the Jacobian, an approximation that is more regional or even global, compared to the linearized local Jacobian used in NSMC. Because of this, ensemble methods can, in general, cope with higher levels of nonlinearity in the relation between parameters and observations and can also scale to much larger numbers of parameters (since the relation between number of parameters and number of model runs is removed).

Although SA-UA-PE methods have been applied numerous times to watershed models such as SWAT (Arnold et al., 1998) (e.g., Pianosi et al., 2017; Nossent et al., 2011; Qiu et al., 2019), their application to coupled surface-subsurface models is sparse (e.g., Herzog et al., 2021; Wu et al., 2014; Ryken et al., 2020). For example, the coupled SWAT-MODFLOW model (Bailey et al., 2016) has been applied to regions worldwide (e.g., Izady et al., 2022; Abbas et al., 2022; Sith et al., 2019); and more recently, the SWAT+ model (Bieger et al., 2017) with the *gwflow* module (Bailey et al., 2020) has been applied to simulate hydrological processes in watershed systems; but these models have been applied without SA and in a deterministic manner, i.e., without including UA. In addition, PE has been challenging, with often SWAT and MODFLOW calibrated separately before being linked, which can be attributed to the complexity in the interaction between SWAT and MODFLOW, as well as the high dimensionality of the parameter space of these two models.

In this paper, we demonstrate the use of SA, PE, and UA methods in a coupled SWAT+*gwflow* model to identify surface and subsurface parameters that control two key watershed responses: streamflow and groundwater head. Hydrologic fluxes in the coupled model include vegetation ET, surface runoff, infiltration, soil percolation and recharge, saturation excess flow, groundwater-stream exchange, soil lateral flow, groundwater pumping, groundwater-lake exchange, tile drainage outflow, and boundary exchange. Targeted parameters include soil properties, evaporation parameters, runoff curve number, snow parameters, aquifer properties (hydraulic conductivity, specific yield), streambed properties (hydraulic conductivity, thickness), and tile drain parameters. The chosen SA method is the Morris screening method, joined to a PE method using the PEST software program (Doherty, 2020). In an alternate method, we demonstrate the use of UA in the PE process, using

an iterative ensemble smooth (iES) to establish prior and posterior ensembles of parameters and system responses. Both methods (PE-SA; iES) can be key components in the application of coupled surface-subsurface models to watershed systems. While in this paper we demonstrate methods for the SWAT+*gwflow* modeling system, they can be applied to other hydrologic models.

We demonstrate the methods for four 8-digit watersheds throughout the conterminous United States: Nanticoke River (Delaware, Maryland), Arkansas Headwaters River (Colorado), Winnebago River (Minnesota, Iowa), and Cache River (Missouri, Arkansas). These watersheds are chosen owing to distinct hydrologic characteristics, such as snowmelt dominant basin (Arkansas Headwaters), shallow groundwater (Nanticoke), the extensive networks of subsurface tile drains (Winnebago), and groundwater pumping for irrigation (Cache). The SWAT+*gwflow* models were simulated for each watershed from 2000 to 2015, with a two-year warm-up period (2000–2001), seven-year calibration period (2002–2008), and seven-year testing period (2009–2015). These models were tested based on annual groundwater head and measured monthly streamflow measured at USGS monitoring wells and stream gages, correspondingly. Preliminary models of SWAT+*gwflow* for the Winnebago River watershed, the Nanticoke River watershed, and the Cache River watershed were presented in Bailey et al. (2023), but only uncalibrated results were provided. This current study establishes possible SA-UA-PE methods to increase model accuracy to a level suitable for scenario analysis (e.g., conservation practices, changes in climate and land use) in these watersheds.

## 2 Materials and Methods

### 2.1 Modeling framework for the study watersheds

Figure 1 presents four watersheds in United States with different hydrologic features were selected for SWAT+*gwflow* simulation: Nanticoke River (Delaware, Maryland), Arkansas Headwaters River (Colorado), Winnebago River (Minnesota, Iowa), and Cache River (Missouri, Arkansas). A comprehensive summary of the primary characteristics of each watershed is presented in Table 1. The annual precipitation rates vary between 425 mm (Arkansas Headwaters) to 1,287 mm (Cache), while the total surface area of the watersheds varies considerably, from 1,787 $km^2$ for Winnebago to 7,940 $km^2$ for Arkansas Headwaters. Each watershed is a headwater 8-digit watershed and is in a different 2-digit region.

These four watersheds were specifically chosen on account of distinctive hydrologic characteristics that demonstrate informative application of the *gwflow*, such as: high baseflow with extensive groundwater discharge to streams (Nanticoke; Wolock, 2003), extensive presence of tile drainage (Winnebago), humid climate (Cache and Nanticoke), semi–arid climate (Arkansas Headwaters), extensive groundwater pumping for irrigation (Cache), and mountain snowmelt (Arkansas Headwaters). A detailed map of study areas showing watershed boundaries, streams, 12-digit catchment boundaries (i.e., subbasin), USGS river gage stations, USGS groundwater monitoring well locations, weather station locations, and water bodies, is shown in Fig. 2.

### 2.1.1 SWAT+ Model

The Soil and Water Assessment Tool (SWAT; Arnold et al., 1998) is a process based, basin scale, semi–distributed, continuous–time hydrologic model that has been applied in many countries around the world for watershed management, policy development, and environmental planning (Bieger et al., 2015; Zhang et al., 2020). The SWAT model was developed and designed by the Agricultural Research Service (ARS) of the United States Department of Agriculture (USDA) to simulate spatial and temporal variations in processes and fluxes of water, nutrients, and sediment. Common uses of the model include assessing water supply, nutrient loads, and sediments loads under historical and future conditions of climate, land use, and land management practices within watersheds and river basins of varying scale (e.g., Ghaffari et al., 2010; Wang et al., 2018; Bhatta et al., 2019). The main computational unit within SWAT is the hydrologic response unit (HRU), unique geographic areas of soil type, land use, and topographic slope (Neitsch et al., 2011), with fluxes aggregated at the subbasin level and then routed to streams. Stream routing occurs from upstream to downstream, with total watershed yield of water, nutrients, and sediment occurring at the watershed outlet.

The SWAT modeling code has recently been restructured to SWAT+ (Bieger et al., 2017), which provides additional flexibility in routing water, nutrients, and sediment between watershed spatial objects (HRUs, aquifers, reservoirs, channels, routing units, wetlands). As an example, fluxes can be routed from HRU to HRU, or from channel to channel within a single subbasin, whereas the original SWAT only allowed routing from HRUs to channels, and each subbasin had a single channel. However, as with the original SWAT model, the groundwater processes are treated simplistically, assuming steady state conditions and homogeneous aquifers, and without physically based movement of groundwater and exchange with surface water features using hydraulic head potential and differences. Hence, the *gwflow* module was created for SWAT+ to allow representation of groundwater processes and fluxes in a physically based manner (Bailey et al., 2020), as described in Section 2.1.2.

In this study, we use SWAT+ models that have been created within the National Agroecosystem Model 'NAM' (White et al., 2022; Arnold et al., 2020), a national effort for improving environmental assessments and conservation strategies. Within the 'NAM', a SWAT + model is constructed for each of the 2,139 HUC8 (8–digit hydrologic unit code) watersheds within the conterminous United States, simulating hydrologic processes and management according to five domains: main rivers (>150 $km^2$), tributaries (15–150 $km^2$), headwaters (1–15 $km^2$), transitions (0.2–2.0 $km^2$), and fields (1–50 ha). Table 2 lists the datasets used to create each SWAT+ model using publicly available data sources. Each cultivated field is designated as a unique HRU, with remaining HRUs delineated based on topographic slope, land use, and soil type. Subbasin boundaries coincide with HUC12 catchments within each HUC8 watershed. Each National Hydrography Dataset (NHD+) channel segment is designated as a unique channel in SWAT+. White et al. (2022) provides detailed information on model construction and input data sets. We use these model set-ups for the four study watersheds.

### 2.1.2 *gwflow* Module

The *gwflow* module (Bailey et al., 2020, 2023) is constructed and combined with SWAT+ for physically based spatially distributed groundwater storage and flow modeling in unconfined aquifer systems, to replace the original SWAT+ groundwater module. The default SWAT+ groundwater module simulates groundwater fluxes with homogeneous aquifer properties, absence of groundwater flow between nearby aquifer systems, and groundwater discharge to streams based on aquifer storage and release parameters, as a substitute to distributed values of gradients and head differences. If the *gwflow* module is activated, the routine is called during each daily time step of the simulation. *gwflow* utilizes a set of grid cells to simulate groundwater storage and flow through time (Fig. 3). Each grid cell has a specified aquifer volume, calculated using the ground surface elevation, bedrock elevation, and specific cell widths. Groundwater storage V ($m^3$) is updated during each daily time step (time *n* to time *n + 1*) for each cell (*i, j*) using a groundwater balance equation:

$$V_{i,j}^{n+1} = V_{i,j}^{n} + (sources_{i,j}^{n} - sinks_{i,j}^{n} \mp lateral\ flow_{i,j}^{n})(t^{n+1} - t^{n}) \quad (1)$$

Sources consist of recharge, stream seepage, and lake seepage; sinks consist of groundwater ET, saturation excess flow, groundwater discharge to streams, pumping, tile drainage outflow, and groundwater discharge to lakes; and lateral flow refers to Darcy flow between adjacent cells, based on cell-specific hydraulic conductivity (*K*) and head gradients. Recharge is provided from HRUs, using a geographic intersection between HRUs and grid cells. Groundwater-stream exchange, groundwater-lake exchange, and tile drainage outflow are calculated with Darcy's Law, using object properties (e.g., streambed conductivity, stream width, stream length). Groundwater pumping can be specified or simulated based on crop irrigation demand, conditioned on available groundwater storage. Once the new volume is calculated, a new value of head is calculated using specific yield ($S_y$) of the grid cell. With the inclusion of the *gwflow* module, SWAT+ simulates land surface, soil, and channel processes, and the *gwflow* module simulates subsurface processes (Fig. 4), with several interface fluxes (soil recharge, saturation excess flow, groundwater-stream exchange, groundwater-lake exchange, tile drainage to streams).

Cell size (m) for the Winnebago, Cache, and Nanticoke watersheds was set at 500 m, whereas cell size for the Arkansas Headwaters, due to a larger spatial extent of the watershed, was set at 1000 m (Table 1). Datasets used to populate *gwflow* cell values (Table 2) include aquifer thickness (ground surface to bedrock; Fig. 5), geologic units for *K* and $S_y$, locations of tile drainage, and USGS groundwater monitoring wells for initial groundwater head in the year 2000. For the latter, spatial interpolation is used between wells to provide a head value for each cell. Cells for groundwater-stream exchange and groundwater-lake exchange are identified by intersecting cells with NHD+ channels and water bodies (see Table 2, Fig. 2), respectively. We note that basic model set-up for the Winnebago, Nanticoke, and Cache watersheds is provided in Bailey et al. (2023), in an initial demonstration of modifying SWAT+ models of the 'NAM' to include the *gwflow* module.

As with the initial set-up of these models, the following features, and limitations of the SWAT+*gwflow* modelling framework, as used in this study, should be noted:

1. The *gwflow* module only considers a single-layer heterogeneous unconfined aquifer, in connection with the network of fields, channels, and reservoirs.
2. Recharge from cultivated fields to the unconfined aquifer is explicitly simulated; however, recharge from non-field HRUs is not spatially explicit, as the delineation of these HRUs is not provided in the 'NAM'. Therefore, recharge for non-field areas is calculated using the average recharge rate for the 12-digit catchment.
3. The *gwflow* module does include an option to move water from the aquifer to the soil profile of the HRU if the water table rises above the base of the soil profile; using this process, shallow groundwater can be used as crop ET or discharged to nearby channels via soil lateral flow. However, due to the lack of spatial representation of non-field HRUs in the 'NAM', the groundwater→soil option is not possible. Therefore, shallow groundwater is allowed to rise to the ground surface and, if groundwater head increases above the ground surface, the volume of water above the ground is routed as saturation excess flow to the nearest channel. We acknowledge this simplification but believe the methods to be adequate in regional-scale applications.
4. Groundwater fluxes along the boundary of the watershed are simulated using a boundary condition approach: the groundwater head in cells along the watershed boundary is assumed to be fixed at the initial value at the beginning of the simulation. If the cell head value is higher than adjacent head values, then groundwater inflow is simulated; if lower, than groundwater outflow is simulated. These fluxes are not calibrated per se, but indirectly as groundwater head values within the watershed are targets in model calibration.

### 2.2 SA-UA-PE Methods for the SWAT+ models

In this section, we describe the application of SA, UA, and PE tools to the watershed models constructed in Section 2.1. The general application of these tools to SWAT+*gwflow* is summarized in the schematic of Fig. 6. In this study, we demonstrate two possible operations: 1) PE with PEST followed by SA with the Morris method, to identify system parameters that control streamflow and groundwater head for each watershed; and 2) PE and UA with iES, to provide prior and posterior ensembles of parameters and system responses (streamflow). The next sections describe the individual tools, and how they are applied to the four watersheds.

#### 2.2.1 Method #1: Parameter ESTimation Tool (PEST) followed by Sensitivity Analysis

The SWAT+*gwflow* models are constructed based on daily time step with 2 years warm-up period (2000–2001), for the calibration period of 2002–2008, and validation period of 2009–2015. SWAT+*gwflow* models are first calibrated and tested using PEST (Doherty, 2020), a nonlinear, model-independent parameter estimator. PEST uses a local optimization technique that utilizes the Gauss-Marquardt-Levenberg algorithm (Doherty, 2004) to minimize the user-defined objective function (e.g., minimization of root mean squares between simulated and observed values). PEST has been broadly employed for sensitivity analysis, uncertainty quantification, and model calibration for water quality and hydrologic models (e.g., Rode et al., 2007; Bahremand and De Smedt, 2010; Jiang et al., 2014).

In this study, we use all available monthly streamflow from USGS stream gage stations and average annual groundwater head from USGS monitoring wells in the objective function ($OF$). There are 1, 2, 3, and 4 stream gaging sites for the Winnebago, Nanticoke, Cache, and Arkansas Headwaters watersheds, respectively, and 7, 26, 92, and 3 monitoring wells (Fig. 2). The contribution of each of these sites to the composite OF were adjusted by manipulating the weights applied to the residuals to ensure that each site is of similar magnitude and significance in determining the optimal parameter values. Local optimization criterion ($LOC$) can be described as the weighted sum of $OF$. Objective function is computed as the squared sum of weighted residuals. $LOC$ and $OF$ can be expressed as:

$$OF = \sum_{j=1}^{n} [x_{j,obs} - x_{j,sim}]^2 \quad (2)$$

$$LOC = \sum_{i=1}^{m} \omega_i \, OF_i \quad (3)$$

where *n* is the total number of the measured/simulated streamflow or groundwater monitoring wells, *m* is the total number of the observation groups of the observed streamflow from the gaging stations and groundwater monitoring wells, and $\omega$ is the weight of the related objective function.

The monthly simulated streamflow of SWAT+*gwflow* models of the four study watersheds is evaluated using determination coefficient ($R^2$), Nash–Sutcliffe Efficiency Index (NSE), Kling–Gupta Efficiency Index (KGE), and percent of bias (PBIAS). The mean absolute error (MAE) is used to evaluate performance of groundwater level at USGS monitoring wells. In our study, we set the maximum number of optimization iterations to 50. However, often PEST converged after 22 iterations (1600 model calls) for Winnebago River, 13 iterations (674 model calls), 36 iterations (2705 model calls) for Arkansas Headwaters, and 13 iterations (843 model calls) for Cache River.

Based on SWAT model literature (e.g., Arnold et al., 2013; Koo et al., 2020), we selected 23 parameters to be modified by PEST (Table 3), focusing on surface runoff, evaporation, soil properties, groundwater processes, and snowmelt accumulation and melt processes. We set 2000–2001 as the warm-up period, 2002–2008 as the calibration period, and 2009–2015 as the testing period. Therefore, in the initial PEST runs, we only use simulation periods of 2000–2008. Once PEST is finished for each watershed model, we then run each model for 2000–2015 to quantify criteria results (i.e., NSE, $R^2$, PBIAS, KGE, and MAE).

Once a parameter set was established using PEST, we applied the Morris screening method to each model to assess the impact of each parameter on streamflow and groundwater head. Morris Screening (Elementary Effects Test) (Morris, 1991) is a qualitative global sensitivity analysis (GSA) technique that computes the relative sensitivity of model parameters, by calculating the change in the model output given a change in the model parameter $x_i$ value (i.e., elementary effect), with all other parameter values held constant. This procedure occurs over a range of parameter values, yielding a relationship between the parameter value and the model output. The following equation demonstrates the computation of a single elementary effect for the $i^{th}$ parameter:

$$EE_i = \frac{f(x_1, \ldots, x_i + \Delta_i, \ldots, x_p) - f(x)}{\Delta_i} \quad (4)$$

where *EEi* is the elementary effect value of the $i^{th}$ model parameter, *f* represents the model, $x_1, \cdots, x_i$ is the model parameter value, and Δ represents the change. Within this method, the mean $\mu$ and standard deviation $\sigma$ of all $EE_i$ for a parameter are often used to assess the sensitivity or significance of parameters. To prevent the canceling of positive and negative values of $EE_i$, Campolongo et al. (2007) proposed using the absolute value of $EE_i$, yielding the mean $\mu^*$. Therefore, $\mu^*$ and $\sigma$ can be calculated as follows for a given parameter $x_i$:

$$\mu_i^* = \frac{1}{n}\sum_{j=1}^{n}|EE_i(j)| \quad (5)$$

$$\sigma_i = \sqrt{\frac{1}{n-1}\sum_{j=1}^{n}\left[EE_i(j) - \frac{1}{n}\sum_{j=1}^{n}EE_i(j)\right]^2} \quad (6)$$

where *n* is the number of $EE_i$ computations. The $\mu^*$ for the model parameters are then ranked, to determine the parameters that have the strongest influence on model output. In this study, we implemented the Morris method using the software tool 'pestpp-sen' (White et al., 2020), variation of PEST. Table 4 lists parameters and their ranges for the four study watersheds. The number of classes (column 3) refers to the number of unique zones or categories for each parameter. For example, for Winnebago River, there are 4 aquifer zones, each with a different value of *K* and $S_y$.

PEST is a powerful inverse modeling tool that can handle many parameters, needs linearity and a stable model, and requires several methods for parameter adjustment. However, determining the minimum of the objective function is restricted if there is a large amount of data error, the model does not represent the data well, and there is a high degree of correlation between the parameters.

### 2.2.2 Method #2: Iterative Ensemble Smoother (iES) for Parameter Estimation and UA

In a second method, we use an iES (Chen and Oliver, 2013) to establish prior and posterior uncertainty estimates of model parameters, within the 'pestpp-ies' (White, 2018) framework that uses the PEST model interface. The iES is based on the original Ensemble Kalman Filter (EnKF) (Evensen, 1994), a data assimilation algorithm that updates state variables through assimilation of measured data into model results, based on correlations between the state variables and the measurement data. For model parameters that have a strong influence on model results, the parameter values can also be updated through this data assimilation. Updates to state variables and parameters occur in a sequence of update steps. The EnKF was implemented in a "smoother" scheme, the Ensemble Smooth (ES) (Van Leeuwen and Evensen, 1996), in which all past states and parameters are updated in a single update step, using all past measurement data. Chen and Oliver (2013) modified the ES to perform iteratively using the Gauss-Levenberg-Marquardt (GLM) algorithm, resulting in a significant decrease in computational burden for models with many parameters.

The iES method starts with an initial ensemble of values for each parameter (i.e., a "prior" ensemble). An estimation to a Jacobian matrix of parameter sensitivities is computed based on the relationships between model parameters and model output, using a range of parameter values based on the prior parameter ensemble (Chen and Oliver, 2013). The contents of the Jacobian matrix are then used to update the ensemble of each model parameter, by seeking to minimize model residuals using the GLM algorithm. The result of the process is a posterior ensemble of model parameters, that are optimally consistent with measured data. Table 4 lists parameters and their ranges used for iES application to the four study watersheds with 3 iterations of the data assimilation algorithm (250 model runs) in 'pestpp-ies'. In general, the data assimilation approach assumes prior and posterior multivariate Gaussian parameter distributions.

## 3 Results and Discussion

We first present hydrologic results for each of the four study watersheds through application of PEST, followed by the results of the Morris sensitivity analysis and the iES application.

### 3.1 Hydrologic State Variables and Fluxes

#### 3.1.1 Streamflow and General Water Balance

The comparison between observed and simulated monthly streamflow at 10 locations showed a good model performance based on NSE, $R^2$, PBIAS, and KGE as presented in Fig. 7 and Table 5 which shows the hydrograph of observed and simulated streamflow at four selected gages. By utilizing desktop computer, an Intel® Core ™ i7-10700 CPU @ 2.90 GHz with 64 GB RAM, simulation times for whole period of simulation (2000–2015) for the four watersheds with SWAT+ and SWAT+*gwflow* are presented in Table 6, ranges (3–13) minutes for base SWAT+ and (7–35) minutes for SWAT+*gwflow*. These fast computation times greatly facilitate calibration, sensitivity analysis, and uncertainty analysis for our regional-scale hydrologic models. Other physically based holistic hydrologic models could be used (e.g., HydroGeoSphere, Parflow, mHM), but required heterogeneous parameters and long computation times are often prohibitive for the hundreds and thousands of simulations runs that are required for the sensitivity analysis and uncertainty analysis conducted in this study.

#### 3.1.2 General Watershed Fluxes

Table 7 displays the annual average hydrologic fluxes for the four study watersheds. Catchment key inflows include groundwater inflow from adjacent aquifer along the catchment boundary and precipitation. Catchment key outputs comprise soil lateral flow, surface runoff, evapotranspiration ET, tile drainage flow, saturation excess flow, and stream seepage.
The internal flows to the watershed include surface water irrigation (calculated by SWAT+), pumping irrigation (computed by *gwflow*), recharge (computed by *gwflow*), and groundwater-reservoir/lake exchange (calculated by *gwflow*). Table 7 also reveals key hydrologic fractions and average annual water yield. Cache has an annual value of (141 mm) for groundwater

pumping for irrigation. Notably, Winnebago has the highest flow of tile drain (62 mm), Nanticoke River demonstrates high fluxes of groundwater to the stream network with saturation excess flow of (183 mm).

Arkansas Headwaters and Cache have small net groundwater discharge to stream (+ 37 Sat excess flow −1.7 mm seepage = + 35.3 mm for cache) and (– 4 mm seepage + 4.6 Sat excess flow = + 0.6 mm for Arkansas Headwaters), owing to deeper groundwater levels in comparison to stream stage. The baseflow contribution is moderate (> 0.30) for Winnebago and Nanticoke Rivers, and low (< 0.20) for the other watersheds. The yield fraction, i.e., the ratio of water yield in the streams to precipitation) ranges from 0.19 (Arkansas Headwaters) to 0.48 (Nanticoke). The recharge fraction ranges from 0.01 (Arkansas Headwaters) to 0.08 (Winnebago), with recharge fluxes for several of the watersheds similar in magnitude to soil lateral flow and surface runoff.

### 3.1.3 Monthly Hydrologic Fluxes

Figure 8 reveals monthly hydrologic flow processes for the period of (2002–2015) for each watershed. Plots on the left show results for the entire watershed system, whereas plots on the right show results for the aquifer system. Key watershed inflows are (boundary inflow and precipitation), where watershed outflows are (tile drainage, groundwater saturation excess flow, runoff, surface ET, and lateral flow) that are showed watershed seasonal fluxes for each basin. The Winnebago River is notable for its high flux rates of tile drainage outflow, groundwater exchange with reservoirs/lakes in the Arkansas Headwaters River, seasonal pattern of saturation excess flow (i.e., groundwater that reaches the river due to groundwater flooding) in the Nanticoke River, and groundwater pumping in the Cache River watershed, exhibiting the unique hydrologic characteristics of each watershed in relation to groundwater storage and flow.

### 3.1.4 Groundwater Head

Figure 9 contains the statistical performance based on mean absolute error (MAE) of annual groundwater level for four study watersheds for the period of 2000–2015. MAE results show an acceptable error (< 1.5 m residual in groundwater level) between simulated and measured average annual groundwater head at each USGS monitoring well site. However, a few locations have higher error (2.5– 3.6 m difference), although these residuals are small compared to the saturated thickness of the aquifer.

### 3.1.5 Spatial Variation of Groundwater Fluxes

Figure 10 shows saturated thickness maps (that is vertical distance between bedrock and water table) for the final year of simulation (2015) for the study watersheds, with saturated thickness similar in spatial pattern to the thickness of the unconfined aquifer (see Figure 5) but differing due to spatial changes in groundwater head within each watershed.

Raster maps of average daily groundwater sink/source flow processes (Fig. 11, 12, and 13) demonstrate zones of stress within the aquifer unit and regions of main inflows into the stream channel system. Spatial fluxes of recharge, groundwater-stream interaction (i.e., saturation excess flow), and groundwater pumping are presented as maps in Fig. 11, Fig. 12, and Fig.

13, respectively. Saturation excess flow occurs where the water table is shallow. Groundwater pumping for irrigation is presented for Nanticoke and Cache, since the other two watersheds do not experience groundwater pumping for irrigation. Cache has the highest pumping rates, due to extensive irrigation practices in the region.

Within the SWAT+*gwflow* framework, stream seepage and groundwater saturation excess runoff constitute groundwater-stream interaction. Throughout the stream system, seepage to the aquifer occurs, with the highest rates typically found along the major rivers because of the large head difference between the stream and the surrounding water table at those locations. High values of saturation excess runoff can be found in the vicinity of rivers and streams in areas of shallow groundwater levels.

### 3.2 Sensitivity Analysis using the Morris Screening Method

The Morris results for parameter influence on streamflow (Fig. 14) show the most influential parameters for each study watershed:

1) For Winnebago: percolation coefficient (Perco1), streambed thickness (bed_thick), hydraulic conductivity of the drain perimeter (tile_k), and streambed hydraulic conductivity (bed_k). These results indicate that streamflow is controlled principally by processes that affect tile drainage and stream-aquifer interactions. This is somewhat surprising, as surface runoff is the dominant flux contributing to streamflow.
2) For Nanticoke: specific yield (syaqu2), hydraulic conductivity (kaqu2), streambed thickness (bed_thick), and streambed hydraulic conductivity (bed_k). These results indicate that groundwater properties and processes control streamflow, in agreement with the high baseflow fraction (0.32) of the watershed (Table 7).
3) For Arkansas Headwaters: Melt factor for snow on June 21 (Mmax), Snowmelt base temperature (Mtmp), streambed thickness (bed_thick), Snowpack temperature lag factor (Tmplag), and curve number (cn_frstgd). This is not surprising, as the streamflow is dominated by spring-time snowmelt patterns.
4) For Cache: Soil evaporation compensation factor (esco), percolation coefficient (Perco2), specific yield (syaqu4), streambed hydraulic conductivity (bed_k), curve number (rcsr_gd), available water capacity (awc3), thickness (bed_thick), Plant uptake compensation factor (epco), and recharge delay (rech_del). Streamflow in this watershed is dominated by processes that affect surface runoff (421 mm in Table 7) and groundwater pumping (141 mm).

Morris results for parameter influence on groundwater level (Fig. 15) show the most influential parameters for each study watershed:

1) For Winnebago: streambed hydraulic conductivity (bed_k), indicating the strong influence of stream-aquifer interactions on groundwater head in the region.
2) For Nanticoke: specific yield (syaqu2) and hydraulic conductivity (kaqu2).
3) For Arkansas Headwaters: hydraulic conductivity (kaqu9) and specific yield (syaqu6).

For Cache: Soil evaporation compensation factor (esco), curve number (rcsr_gd), and available water capacity (awc3 and awc4), indicating the influence of land surface and soil processes on groundwater head, due to their control on the volume of groundwater that is pumped from the aquifer.

The estimated time-varying parameter sensitivity calculated by the Morris method are represented in Fig. 16 for the most influential parameters in the four watersheds. These values are a combination of streambed parameters (bed_k), soil parameters (perc1, esco), snow parameters (Mmax, Mtmp), and aquifer parameters (syaqu2, kaqu2), depending on the watershed. The Nanticoke River model is dominated by aquifer parameters due to shallow groundwater levels and associated groundwater discharge to the stream network. The Arkansas River model is dominated by snow parameters due to mountainous terrain in the Rocky Mountains. These results indicate that these parameters have a seasonal fluctuation in their influence on streamflow, due to the seasonal fluctuations and timing of groundwater levels, snowfall, and crop growth.

The strong influence of streambed parameters (streambed conductivity, streambed thickness) on system responses in each of the four study watersheds is expected due to the coupled surface/subsurface nature of the watersheds. Water exchange between channels and aquifers increases with increasing conductivity and decreasing thickness. Streambed parameters have a strong control on streamflow for each of the four watersheds, whereas they control groundwater head for only the Winnebago River watershed and the Nanticoke River watershed, due to shallow groundwater levels in relation to ground surface and channel elevation. For streamflow, control is either in the direction of channel→aquifer (seepage) or aquifer→channel (discharge). For the Cache River watershed, extensive groundwater pumping (see Figure 13) can lead to enhanced stream seepage ("streamflow depletion") which, as noted by previous studies (Fox and Durnford, 2003; Fox, 2007) can be sensitive to streambed conductivity. In general, the importance of streambed parameters such as conductivity and thickness in the modeling of surface-groundwater (SW-GW) exchange fluxes have been noted extensively (Kalbus et al., 2009; Brunner et al., 2017; Partington et al., 2017), with many studies aimed at quantifying these parameters spatially (e.g., Fox, 2007; Crook et al., 2008; Wojnar et al., 2013; Shi and Wang, 2023).

### 3.3 Uncertainty Analysis and Parameter Estimation using the iES

Figure 17 shows the observed and best estimated monthly streamflow with prior and posterior prediction uncertainty band for the four study watersheds. The plots in the left column represent prior parameter ensembles (uncalibrated Monte Carlo results) with wide uncertainty bands. Meanwhile, the plots in the right column show the posterior ensemble that effectively reduces the uncertainty band. For example, in Arkansas Headwaters, the prior ensemble uncertainty band was shifted to the left of the measured streamflow, owing to an incorrect characterization of snowmelt timing and magnitude. However, the posterior ensemble uncertainty band is much narrower and fits the timing and magnitude of the measured streamflow.

Figure 18 demonstrates the effect of data assimilation on the parameters more quantitatively, which compares the histogram of prior parameter ensembles (gray), with the histogram of posterior parameter ensembles (blue), for 9 of the most influential parameters in the four study watersheds. The posterior distribution of parameters is narrower than the prior distribution,

which helps in the estimation of model parameters. The range parameters for curve number–Cache River (Fig. 18–H) and specific yield–Nanticoke River (Fig. 18–C) indicate the largest influence of data assimilation. Short correlation ranges have been reduced from the posterior.

Figure 19 shows the influence of data assimilation on the average annual water balance more quantitatively, which compares the histogram of prior ensembles (gray), with the histogram of posterior ensembles (blue), for 8 most important water balance components in the four study watersheds. The posterior distribution of parameters is narrower than the prior distribution, which helps in the estimation of water balance component.

In general, the application of the iES can provide ensembles of posterior parameter sets that, when used in the model, provide simulation results that are in close comparison with measured data. And, due to the use of ensembles, includes uncertainty in results. When used for scenario analysis and decision making, these models can employ the posterior ensembles of parameters to propagate uncertainty into model results, therefore serving effectively in the role of decision support.

In general, ensemble-based data assimilation naturally accommodates parameter correlation, both in the prior parameter distribution (as expressed in the prior parameter covariance matrix), as well as correlations between parameters that give correlated responses to historic observations. The former is addressed simply by providing the requisite covariance matrix or by generating a prior parameter ensemble that is imbued with appropriate parameter relations. The latter correlations, those typically referred as non-uniqueness, are handled algorithmically through the truncated SVD solution to as a mechanism to stable is the inverse problem, as well as implicitly through the use of an ensemble that is naturally rank deficient (in that it does not fully occupy the range space of the parameter space). The rank deficient ensemble used to approximate the Jacobian matrix only occupies the dominant singular components of the full Jacobian – these dominate singular components are a subspace the includes the parameter combinations that represent parameters that are nonunique with respect to the historical observations. It is worth noting one of the strengths of an ensemble-based approach to history matching is that the posterior parameter spans this non-uniqueness. Results for stand-alone SWAT+ models, i.e., models without the *gwflow* module included, are provided in Supporting Information.

## 4 Summary and Conclusions

In this article, we present two methods to include sensitivity analysis, uncertainty analysis, and parameter optimization into coupled surface-subsurface hydrologic models, using the SWAT+ model as an example. The method utilizes the *gwflow* module, which is a spatially distributed, physically based groundwater flow module coupled to the SWAT+ model, which utilizes aquifer control volumes (i.e., grid cells) to compute daily water balance in an unconfined aquifer. We present our technique for four different U.S. watersheds: Winnebago River, Nanticoke River, Cache River, and Arkansas Headwaters. These watersheds were selected on account of their respective unique hydrologic features: an extensive network of tile drain

(Winnebago), shallow groundwater (Nanticoke), snow-melt dominant (Arkansas Headwaters), and extensive groundwater pumping for irrigation (Cache).

The SWAT+*gwflow* models are calibrated based on the monthly streamflow and annual groundwater level for the period of 2000–2008 with 2-years warm-up period, validated for a period of 2009–2015. The parameter estimation software (PEST) and (PEST++) are used for the calibration, sensitivity analysis, and uncertainty analysis of hydrologic models. Additionally, watershed water balance fluxes are evaluated for stability of models. All watershed models showed good statistical performance of streamflow simulation (10 River gages locations) and groundwater level results (128 monitoring wells), however, a few wells exhibited high values of mean absolute error results. Model outputs comprising saturated thickness (spatial maps), raster maps of groundwater flow processes (saturation excess flow, stream seepage, pumping, recharge) which can be utilized to validate the model and recognize areas that need further parameter estimation, groundwater head (time series and spatial maps of observation locations), and stream discharge. By combining average annual water balance fluxes, groundwater head, and streamflow data, hydrologic flow processes can be restricted to realistic ranges. Increased fidelity in process representation allows these modeling tools to be utilized for the assessment of water resources under different land use and climate scenarios over a wide range of hydrologic conditions.

GSA using Morris screening technique was applied to SWAT+*gwflow* models of study watersheds to assess the governing system factors on surface runoff and groundwater fluxes. The 'pestpp-sen' tool within the PEST++ environment is utilized to generate parameter values, update model files for SWAT+*gwflow* models, run the model simulations, and compute sensitivity indices for the Morris method. The sensitivity of 23 parameters (including surface runoff fluxes, actual and potential evapotranspiration fluxes, groundwater flow fluxes, snow fluxes, and soil water fluxes) were investigated based on 2 model responses: minimizing monthly streamflow and minimizing the mean absolute error (MAE) of annual groundwater head data.

The iES method was used for the model input uncertainty for the prior (uncalibrated results) and posterior ensembles, thus, resulting in better uncertainty prediction that will improve the utilize of hydrologic models in decision-making. This technique is implemented using 'pestpp-ies' tool within the PEST++ environment.

From the results we conclude that:

1) Winnebago River (extensive presence of tile drainage): groundwater flow-related parameters and soil water parameters significantly affect streamflow and groundwater heads, especially percolation coefficient, streambed thickness, hydraulic conductivity of the drain perimeter, and streambed hydraulic conductivity.
2) Nanticoke River (intensive surface–groundwater interaction): groundwater flow-related parameters notably influence streamflow and groundwater heads, specifically specific yield, hydraulic conductivity, streambed thickness, and streambed hydraulic conductivity.
3) Arkansas Headwaters River (snowmelt dominant basin): Snow processes and surface runoff flow related parameters extensively affect streamflow. While groundwater flow parameters significantly influence groundwater heads. Snow parameters include Melt factor for snow on June 21, Snowmelt base temperature, streambed thickness,

Snowpack temperature lag factor, and curve number for surface runoff processes. Groundwater flow parameters hydraulic conductivity and specific yield.

4) Cache River (extensive groundwater pumping for irrigation): soil water related parameters significantly affect streamflow including Soil evaporation compensation factor and percolation coefficient. Meanwhile, groundwater flow and surface runoff have parameters a relatively less influence on stream discharge. For groundwater head, soil water related parameters pointedly affect streamflow comprising available water capacity and Soil evaporation compensation factor.

5) The iES method represents prior parameter ensembles (uncalibrated Monte Carlo results) with wide uncertainty band, and the posterior ensemble effectively reduces the uncertainty band. This technique can give best estimation parameter ranges, water balance components, and simulated streamflow and groundwater heads.

While these SA-UA-PO methods have been demonstrated here for the SWAT+*gwflow* model, they can be applied generally to other coupled surface-subsurface models, or even stand-alone watershed models such as SWAT or SWAT+.

**Acknowledgements**

The United States Department of Agriculture–Agricultural Research Service provided funding for this study through Cooperative Agreements 59-3098-8-002 and 59-3098-2-001.USDA is an Equal Opportunity Employer and Provider.

**Author contributions:**

The research was designed by S.A., R.B., and J.W., with model coding performed by R.B., J.W., and J.A. S.A., R.B., J.W., M.W., J.A., N.C., and J.G. conducted the research, and R.B., S.A., J.G., and N.C. analyzed the data. The paper was written by S.A., R.B., J.W, and M.W.

**Conflicts of Interest**

The authors declare no conflict of interest.

**References**

Abbas, S., Xuan, Y., and Bailey, R.: Assessing Climate Change Impact on Water Resources in Water Demand Scenarios Using SWAT-MODFLOW-WEAP. *Hydrology*, *9*(10), 164. https://doi.org/10.3390/hydrology9100164, 2022.

Arnold, J., Kiniry, J., Srinivasan, R., Williams, J., Haney, E., and Neitsch, S.: Soil & Water Assessment Tool: Input/output documentation. version 2012. Texas Water Resources Institute 2013 TR-439. https://swat.tamu.edu/media/69296/swat-io-documentation-2012.pdf, 2013.

Arnold, J., Srinivasan, R., Muttiah, R., and Williams, J.: Large area hydrologic modeling and assessment part I: Model development. *J. Am. Water Resour. As.*, *34*(1), 73-89. https://doi.org/10.1111/j.1752-1688.1998.tb05961.x, 1998.

Arnold, J., White, M., Allen, P., Gassman, P., and Bieger, K.: Conceptual Framework of connectivity for a national agroecosystem model based on transport processes and management practices. *J. Am. Water Resour. As.*, *57*(1), 154-169. https://doi.org/10.1111/1752-1688.12890, 2020.

Bahremand, A., and De Smedt, F.: Predictive Analysis and Simulation Uncertainty of a Distributed Hydrological Model. *Water Resour. Manage.*, *24*, 2869–2880. https://doi.org/10.1007/s11269-010-9584-1, 2010.

Bailey, R., Wible, T., Arabi, M., Records, R., and Ditty, J.: Assessing regional-scale spatio-temporal patterns of groundwater-surface water interactions using a coupled SWAT-MODFLOW model. *Hydrol. Process.*, *30*(23), 4420-4433. https://doi.org/10.1002/hyp.10933, 2016.

Bailey, R., Abbas, S., Arnold, J., White, M., Gao, J., and Čerkasova, N.: Augmenting the national agroecosystem model with physically based spatially distributed groundwater modeling. *Environ. Model. SoftW.*, *160*, 105589. https://doi.org/10.1016/j.envsoft.2022.105589, 2023.

Bailey, R., and Alderfer, C.: Groundwater Data in Unconfined Aquifers - conterminous United States. *figshare*. Collection. https://doi.org/10.6084/m9.figshare.c.5918738.v2, 2022.

Bailey, R., Bieger, K., Arnold, J., and Bosch, D.: A new physically-based spatially-distributed groundwater flow module for SWAT+. *Hydrology*, *7*(4), 75. https://doi.org/10.3390/hydrology7040075, 2020.

Bailey, R., Bieger, K., Flores, L., and Tomer, M.: Evaluating the contribution of subsurface drainage to watershed water yield using SWAT+ with groundwater modeling. *Sci. Total Environ.*, *802*, 149962. https://doi.org/10.1016/j.scitotenv.2021.149962, 2022.

Bennett, N., Croke, B., Guariso, G., Guillaume, J., Hamilton, S., Jakeman, A., *et al.*: Characterising performance of environmental models. *Environ. Model. SoftW.*, *40*, 1-20. https://doi.org/10.1016/j.envsoft.2012.09.011, 2013.

Bhatta, B., Shrestha, S., Shrestha, P., and Talchabhadel, R.: Evaluation and application of a SWAT model to assess the climate change impact on the hydrology of the Himalayan River Basin. *Catena*, *181*, 104082. https://doi.org/10.1016/j.catena.2019.104082, 2019.

Bieger, K., Arnold, J., Rathjens, H., White, M., Bosch, D., Allen, P., *et al.*: Introduction to SWAT+, a completely restructured version of the soil and water assessment tool. *J. Am. Water Resour. As.*, *53*(1), 115-130. https://doi.org/10.1111/1752-1688.12482, 2017.

Bieger, K., Hörmann, G., and Fohrer, N.: Detailed spatial analysis of SWAT-simulated surface runoff and sediment yield in a mountainous watershed in China. *Hydrol Sci J.*, *60*(5), 784-800. https://doi.org/10.1080/02626667.2014.965172, 2015.

Bieger, K., Rathjens, H., Arnold, J., Chaubey, I., and Allen, P.: Development and comparison of multiple regression models to predict bankfull channel dimensions for use in hydrologic models. *J. Am. Water Resour. As.*, *52*(6), 1385-1400. https://doi.org/10.1111/1752-1688.12460, 2016.

Bocquet, M., and Sakov, P.: An iterative ensemble Kalman smoother. *Q. J. R. Meteorol. Soc.*, *140*(682), 1521-1535. https://doi.org/10.1002/qj.2236, 2014.

Brunner, P., Therrien, R., Renard, P., Simmons, C., and Franssen, H.: Advances in understanding river-groundwater interactions. *Rev. Geophys.*, *55*(3), 818-854. https://doi.org/10.1002/2017RG000556, 2017.

Campolongo, F., Cariboni, J., and Saltelli, A.: An effective screening design for sensitivity analysis of large models. *Environ. Model. SoftW.*, *22*(10), 1509-1518. https://doi.org/10.1016/j.envsoft.2006.10.004, 2007.

Čerkasova, N., Umgiesser, G., and Ertürk, A.: Modelling framework for flow, sediments and nutrient loads in a large transboundary river watershed: A climate change impact assessment of the Nemunas river watershed. *J. Hydrol*, *598*, 126422. https://doi.org/10.1016/j.jhydrol.2021.126422, 2021.

Chen, Y., and Oliver, D.: Ensemble randomized maximum likelihood method as an iterative ensemble smoother. *Math. Geosci.*, *44*, 1-26. https://doi.org/10.1007/s11004-011-9376-z, 2012.

Chen, Y., and Oliver, D.: Levenberg–Marquardt forms of the iterative ensemble smoother for efficient history matching and uncertainty quantification. *Comput. Geosci.*, *17*(4), 689-703. https://doi.org/10.1007/s10596-013-9351-5, 2013.

Chen, Y., and Oliver, D.: Localization and regularization for iterative ensemble smoothers. *Comput. Geosci.*, *21*(1), 13-30. https://doi.org/10.1007/s10596-016-9599-7, 2017.

Crestani, E., Camporese, M., Baú, D., and Salandin, P.: Ensemble Kalman filter versus ensemble smoother for assessing hydraulic conductivity via tracer test data assimilation. *Hydrol Earth Syst Sci.*, *17*(4), 1517-1531. https://doi.org/10.5194/hess-17-1517-2013, 2013.

Crook, N., Binley, A., Knight, R., Robinson, D., Zarnetske, J., and Haggerty, R.: Electrical resistivity imaging of the architecture of substream sediments. *Water Resour. Res.*, *44*(4). https://doi.org/10.1029/2008WR006968, 2008.

Devak, M., and Dhanya, C.: Sensitivity analysis of hydrological models: Review and way forward. *J. Water Clim.*, *8*(4), 557-575. https://doi.org/10.2166/wcc.2017.149, 2017.

Dieter, C., Maupin, M., Caldwell, R., Harris, M., Ivahnenko, T., Lovelace, J., Barber, N., and Linsey, K.: *Water availability and use science program: Estimated use of water in the United States in 2015* (Circular 1441). US Geological Survey. https://doi.org/10.3133/cir1441, 2018.

Doherty, J., and Hunt, R.: Two statistics for evaluating parameter identifiability and error reduction. *J. Hydrol*, *366*(1-4), 119-127. https://doi.org/10.1016/j.jhydrol.2008.12.018, 2009.

Doherty, J.: PEST model-independent parameter estimation user manual. *Watermark Numerical Computing, Brisbane, Australia*, *3338*, 3349, 2004.

Doherty, J.: PEST, Model-independent Parameter Estimation: User Manual (seventh ed.). *Watermark Numerical Computing, Brisbane, Australia*, *3338*, 3349, 2020.

Evensen, G.: Sequential data assimilation with a nonlinear quasi-geostrophic model using Monte Carlo methods to forecast error statistics. *J. Geophys. Res.: Oceans*, *99*(C5), 10143-10162. https://doi.org/10.1029/94JC00572, 1994.

Fox, G., and Durnford, D.: Unsaturated hyporheic zone flow in stream/aquifer conjunctive systems. *Adv. Water Resour.*, *26*(9), 989-1000. https://doi.org/10.1016/S0309-1708(03)00087-3, 2003.

Fox, G.: Estimating streambed conductivity: guidelines for stream-aquifer analysis tests. *Trans ASABE*, *50*(1), 107-113. https://doi.org/10.13031/2013.22416, 2007.

Gesch, D., Evans, G., Oimoen, M., and Arundel, S.: The national elevation dataset (pp. 83–110). American Society for Photogrammetry and Remote Sensing, 2018.

Ghaffari, G., Keesstra, S., Ghodousi, J., and Ahmadi, H.: SWAT-simulated hydrological impact of land-use change in the Zanjanrood basin, Northwest Iran. *Hydrol. Process.*, *24*(7), 892-903. https://doi.org/10.1002/hyp.7530, 2010.

Helton, J.: Uncertainty and sensitivity analysis techniques for use in performance assessment for Radioactive Waste Disposal. *Reliab. Eng. Syst. Saf.*, 42(2-3), 327-367. https://doi.org/10.1016/0951-8320(93)90097-i, 1993.

Herzog, A., Hector, B., Cohard, J., Vouillamoz, J., Lawson, F. M., Peugeot, C., and De Graaf, I.: A parametric sensitivity analysis for prioritizing regolith knowledge needs for modeling water transfers in the West African critical zone. *Vadose Zone J.*, *20*(6), e20163. https://doi.org/10.1002/vzj2.20163, 2021.

Horton, J., San Juan, C., and Stoeser, D.: *The state geologic map compilation (SGMC) geodatabase of the conterminous United States, ver. 1.1, August 2017* (Data Series 1052). https://doi.org/10.3133/ds1052, 2017.

Izady, A., Joodavi, A., Ansarian, M., Shafiei, M., Majidi, M., Davary, K., *et al.*: A scenario-based coupled SWAT-MODFLOW decision support system for Advanced Water Resource Management. *J. Hydroinform.*, 24(1), 56-77. https://doi.org/10.2166/hydro.2021.081, 2022.

Jiang, S., Jomaa, S., and Rode, M.: Modelling inorganic nitrogen leaching in nested mesoscale catchments in central Germany. *Ecohydrology*, *7*(5), 1345-1362. https://doi.org/10.1002/eco.1462, 2014.

Kalbus, E., Schmidt, C., Molson, J. W., Reinstorf, F., and Schirmer, M.: Influence of aquifer and streambed heterogeneity on the distribution of groundwater discharge. *Hydrol. Earth Syst. Sci.*, *13*(1), 69-77. https://doi.org/10.5194/hess-13-69-2009, 2009.

Koo, H., Chen, M., Jakeman, A., and Zhang, F.: A global sensitivity analysis approach for identifying critical sources of uncertainty in non-identifiable, spatially distributed environmental models: A holistic analysis applied to SWAT for input datasets and model parameters. *Environ. Model. SoftW.*, *127*, 104676. https://doi.org/10.1016/j.envsoft.2020.104676, 2020.

Leta, O., Nossent, J., Velez, C., Shrestha, N., Van Griensven, A., and Bauwens, W.: Assessment of the different sources of uncertainty in a SWAT model of the River Senne (Belgium). *Environ. Model. SoftW.*, 68, 129-146. https://doi.org/10.1016/j.envsoft.2015.02.010, 2015.

Liu, H., Jia, Y., Niu, C., Su, H., Wang, J., Du, J., *et al.*: Development and validation of a physically-based, national-scale hydrological model in China. *J. Hydrol.*, *590*, 125431. https://doi.org/10.1016/j.jhydrol.2020.125431, 2020.

Moore, R., and Dewald, T.: The road to nhdp lus — advancements in digital stream networks and associated catchments. *J. Am. Water Resour. As.*, *52*(4), 890-900. https://doi.org/10.1111/1752-1688.12389, 2016.

Morris, M.: Factorial sampling plans for preliminary computational experiments. *Technometrics*, *33*(2), 161-174. https://doi.org/10.2307/1269043, 1991.

Neitsch, S., Arnold, J., Kiniry, J., and Williams, J.: *Soil and Water Assessment Tool Theoretical Documentation version 2009*. Texas Water Resources Institute. https://swat.tamu.edu/media/99192/swat2009-theory.pdf, 2011.

Nossent, J., Elsen, P., and Bauwens, W.: Sobol' sensitivity analysis of a complex environmental model. *Environ. Model. SoftW.*, *26*(12), 1515-1525. https://doi.org/10.1016/j.envsoft.2011.08.010, 2011.

Olaya-Abril, A., Parras-Alcántara, L., Lozano-García, B., and Obregón-Romero, R.: Soil Organic Carbon Distribution in Mediterranean areas under a climate change scenario via multiple linear regression analysis. *Sci. Total Environ.*, *592*, 134-143. https://doi.org/10.1016/j.scitotenv.2017.03.021, 2017.

Partington, D., Therrien, R., Simmons, C., and Brunner, P.: Blueprint for a coupled model of sedimentology, hydrology, and hydrogeology in streambeds. *Rev. Geophys.*, *55*(2), 287-309. https://doi.org/10.1002/2016RG000530 , 2017.

Pianosi, F., Iwema, J., Rosolem, R., and Wagener, T.: A multimethod global sensitivity analysis approach to support the calibration and evaluation of Land Surface Models. *Sensitivity Analysis in Earth Observation Modelling*, 125-144. https://doi.org/10.1016/b978-0-12-803011-0.00007-0, 2017.

Plischke, E., Borgonovo, E., and Smith, C.: Global sensitivity measures from given data. *European Eur. J. Oper. Res.*, *226*(3), 536-550. https://doi.org/10.1016/j.ejor.2012.11.047, 2013.

Pokhrel, Y., Felfelani, F., Satoh, Y. *et al.*: Global terrestrial water storage and drought severity under climate change. *Nat. Clim. Chang.*, *11*, 226–233. https://doi.org/10.1038/s41558-020-00972-w, 2021.

Qiu, J., Yang, Q., Zhang, X., Huang, M., Adam, J. C., and Malek, K.: Implications of water management representations for watershed hydrologic modeling in the Yakima River Basin. *Hydrol Earth Syst Sci.*, *23*(1), 35-49. https://doi.org/10.5194/hess-23-35-2019, 2019.

Rode, M., Suhr, U., and Wriedt, G.: Multi-objective calibration of a river water quality model—Information content of calibration data. *Ecol. Modell.*, *204*(1-2), 129-142. https://doi.org/10.1016/j.ecolmodel.2006.12.037, 2007.

Ryken, A., Bearup, L., Jefferson, J., Constantine, P., and Maxwell, R.: Sensitivity and model reduction of simulated snow processes: Contrasting observational and parameter uncertainty to improve prediction. *Adv. Water Resour.*, *135*, 103473. https://doi.org/10.1016/j.advwatres.2019.103473, 2020.

Santos, L., Andersson, J., and Arheimer, B.: Evaluation of parameter sensitivity of a rainfall-runoff model over a global catchment set. *Hydrol Sci J.*, *67*(3), 342-357. https://doi.org/10.1080/02626667.2022.2035388, 2022.

Shangguan, W., Hengl, T., Mendes de Jesus, J., Yuan, H., and Dai, Y.: Mapping the global depth to bedrock for land surface modeling. *J. Adv. Model. Earth Syst.*, *9*(1), 65-88. https://doi.org/10.1002/2016ms000686, 2017.

Shi, W., and Wang, Q.: An Analytical Model of Multi-layered Heat Transport to Estimate Vertical Streambed Fluxes and Sediment Thermal Properties. *J. Hydrol.*, 129963. https://doi.org/10.1016/j.jhydrol.2023.129963, 2023.

Sith, R., Watanabe, A., Nakamura, T., Yamamoto, T., and Nadaoka, K.: Assessment of water quality and evaluation of best management practices in a small agricultural watershed adjacent to Coral Reef area in Japan. *Agric. Water Manag.*, *213*, 659-673. https://doi.org/10.1016/j.agwat.2018.11.014, 2019.

Skinner, K., and Maupin, M.: *Point-source nutrient loads to streams of the conterminous United States, 2012* (No. 1101). US Geological Survey. https://doi.org/10.3133/ds1101, 2019.

Soil Survey Staff: Gridded soil survey geographic (gSSURGO) database for the conterminous United States, 2014.

Valayamkunnath, P., Barlage, M., Chen, F., Gochis, D., and Franz, K.: Mapping of 30-meter resolution tile-drained croplands using a geospatial modeling approach. *Sci. Data*, *7*(1), 257. https://doi.org/10.1038/s41597-020-00596-x, 2020.

Van Leeuwen, P., and Evensen, G.: Data assimilation and inverse methods in terms of a probabilistic formulation. *Mon. Weather Rev.*, *124*(12), 2898-2913. https://doi.org/10.1175/1520-0493(1996)124<2898:DAAIMI>2.0.CO;2, 1996.

Wang, Y., Bian, J., Zhao, Y., Tang, J., and Jia, Z.: Assessment of future climate change impacts on nonpoint source pollution in snowmelt period for a cold area using SWAT. *Sci. Rep.*, *8*(1), 1-13. https://doi.org/10.1038/s41598-018-20818-y, 2018.

Wei, X., Bailey, R., and Tasdighi, A.: Using the SWAT model in intensively managed irrigated watersheds: Model modification and Application. *J. Hydrol. Eng.*, *23*(10). https://doi.org/10.1061/(asce)he.1943-5584.0001696, 2018.

White, J., Hunt, R., Fienen, M., and Doherty, J.: Approaches to Highly Parameterized Inversion: PEST++ Version 5, a Software Suite for Parameter Estimation, Uncertainty Analysis, Management Optimization and Sensitivity Analysis: U.S. Geological Survey Techniques and Methods 7C26, 52 p., https://doi.org/10.3133/tm7C26, 2020.

White, J.: A model-independent iterative ensemble smoother for efficient history-matching and uncertainty quantification in very high dimensions. *Environ. Model. SoftW.*, *109*, 191-201. https://doi.org/10.1016/j.envsoft.2018.06.009, 2018.

White, M., Arnold, J., Bieger, K., Allen, P., Gao, J., Čerkasova, N., *et al.*: Development of a field scale SWAT+ Modeling Framework for the contiguous U.S. *J. Am. Water Resour. As.*, *58*(6), 1545-1560. https://doi.org/10.1111/1752-1688.13056, 2022.

Wojnar, A., Mutiti, S., and Levy, J.: Assessment of geophysical surveys as a tool to estimate riverbed hydraulic conductivity. *J. Hydrol.*, *482*, 40-56. https://doi.org/10.1016/j.jhydrol.2012.12.018, 2013.

Wolock, D. M.: *Base-flow index grid for the conterminous United States* (No. 2003-263). https://doi.org/10.3133/ofr03263, 2003.

Wu, B., Zheng, Y., Tian, Y., Wu, X., Yao, Y., Han, F., et. al.: Systematic assessment of the uncertainty in integrated surface water-groundwater modeling based on the probabilistic collocation method. *Water Resour. Res.*, *50*(7), 5848-5865. https://doi.org/10.1002/2014WR015366 , 2014.

Wu, J., Yen, H., Arnold, J., Yang, Y., Cai, X., White, M., *et al.*: Development of reservoir operation functions in SWAT+ for national environmental assessments. *J. Hydrol.*, *583*, 124556. https://doi.org/10.1016/j.jhydrol.2020.124556, 2020.

655 Yan, L., and Roy, D.: Conterminous United States crop field size quantification from multi-temporal Landsat Data. *Remote Sensing of Environment*, *172*, 67-86 https://doi.org/10.1016/j.rse.2015.10.034, 2016.

Zhang, H., Wang, B., Li Liu, D., Zhang, M., Leslie, L. M., and Yu, Q.: Using an improved SWAT model to simulate hydrological responses to land use change: A case study of a catchment in tropical Australia. *J. Hydrol.*, *585*, 124822. https://doi.org/10.1016/j.jhydrol.2020.124822, 2020.

660

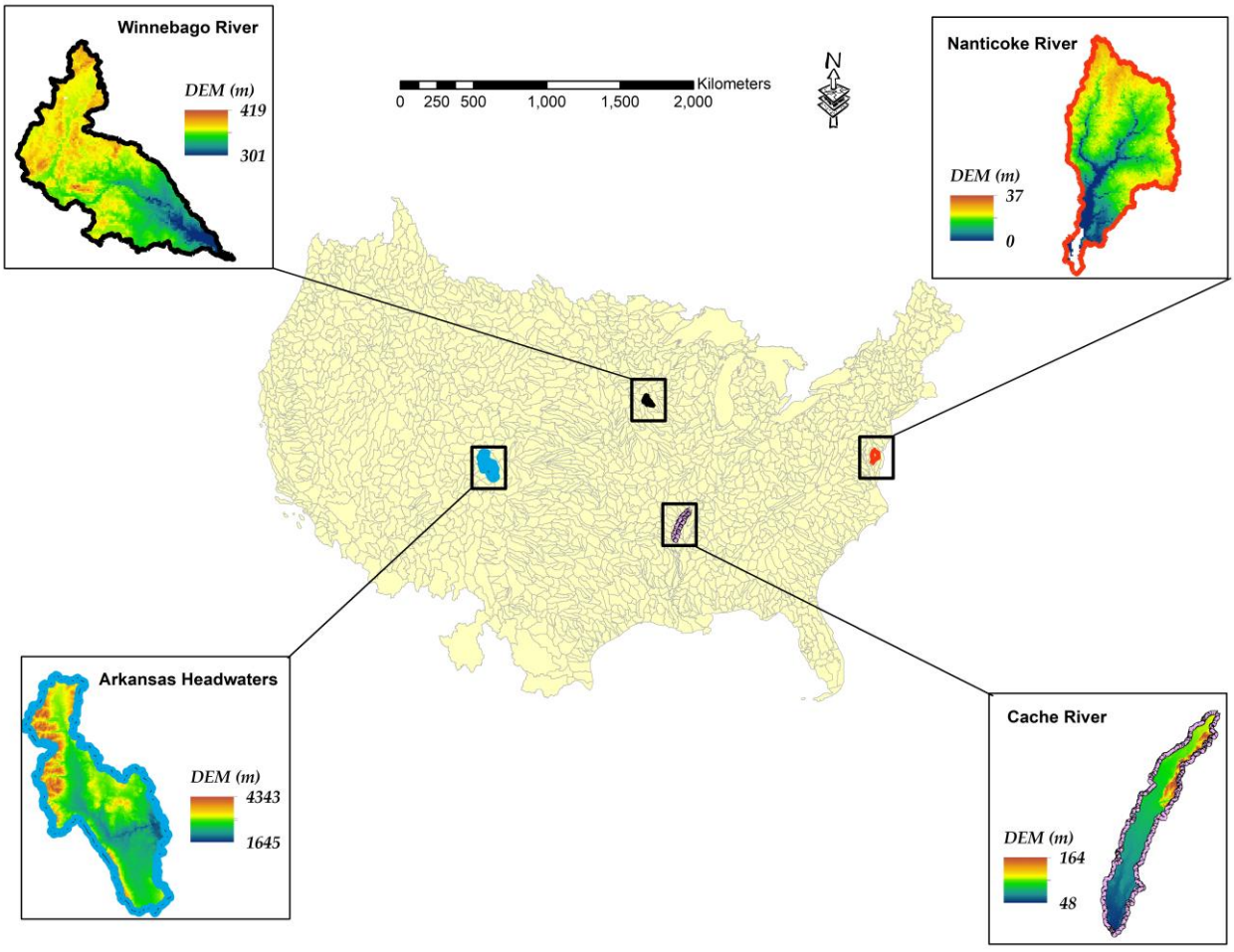


665 **Figure 1: Geographical locations, and digital elevation model of the four study watersheds. Arkansas Headwaters River; Winnebago River; Nanticoke River; and Cache River.**

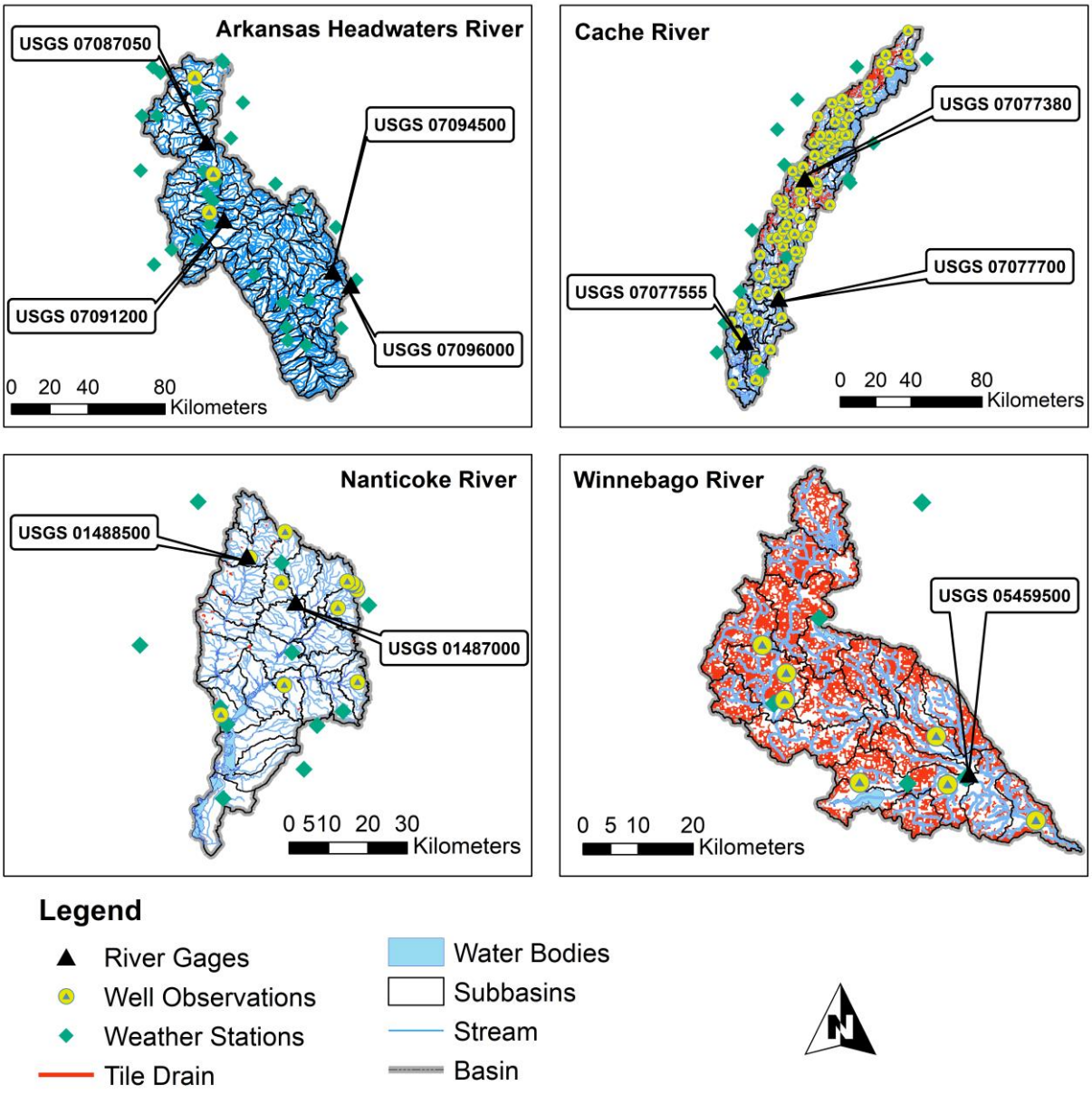


**Figure 2: Detailed maps of the study watersheds, revealing the location of water bodies, streams, USGS monitoring wells, weather stations, subbasin boundaries, tile drains, and river gages stations.**

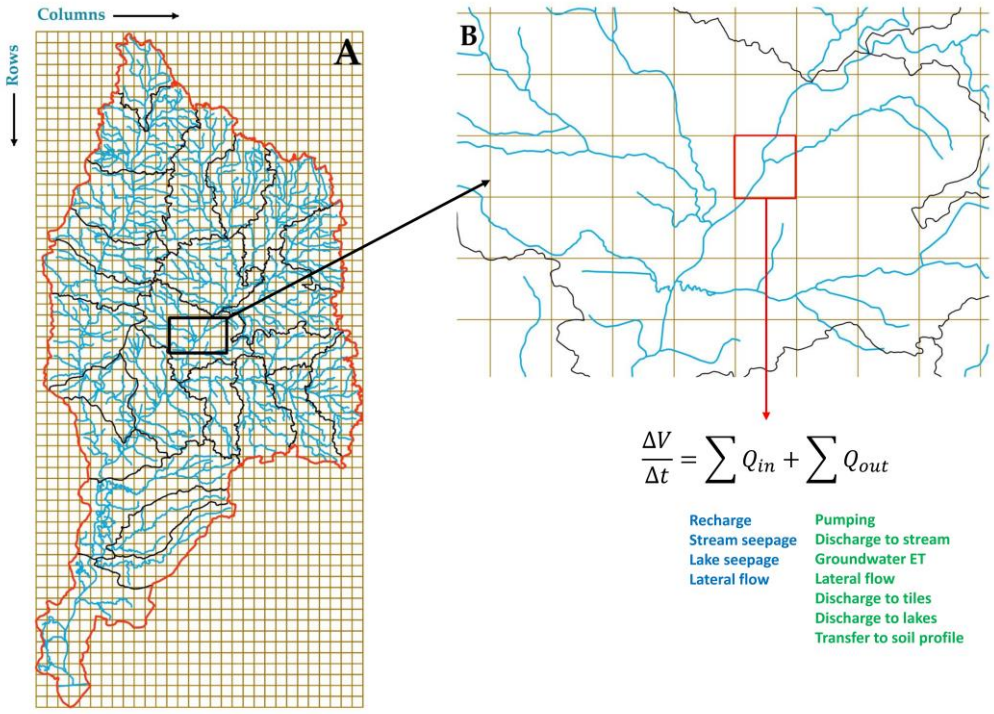


**Figure 3: Geographical layout and computation method of the *gwflow* module, presenting (A) grid cells, watershed boundary (red line), stream channels (blue lines), and subbasins (black lines) for the Nanticoke watershed; and (B) Zoomed-in of channels and grid, demonstrating the water balance computations for each cell.**

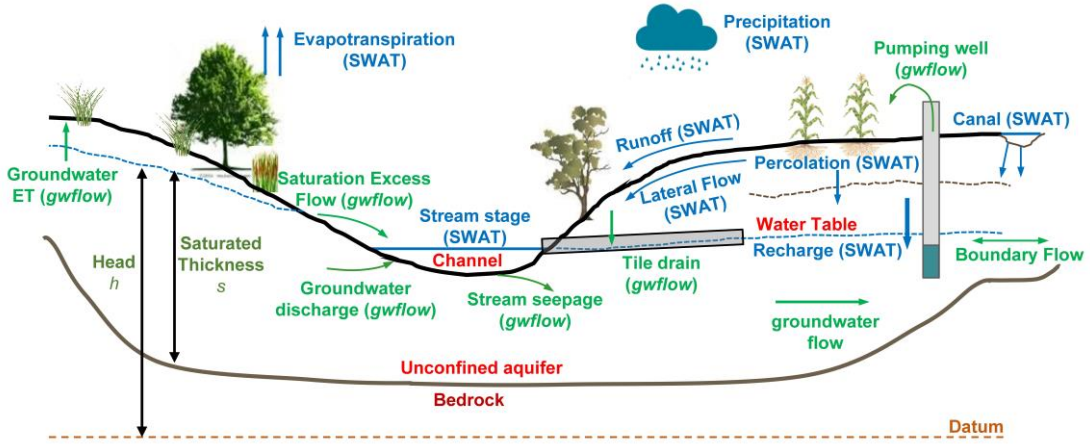


675

**Figure 4: Schematics representation of the hydrologic processes in a typical watershed stream-aquifer system showing main hydrologic elements and hydrologic processes for SWAT+ and *gwflow*. Blue arrows outline fluxes that are calculated by SWAT+, green arrows for flow processes that are computed by *gwflow*.**

680

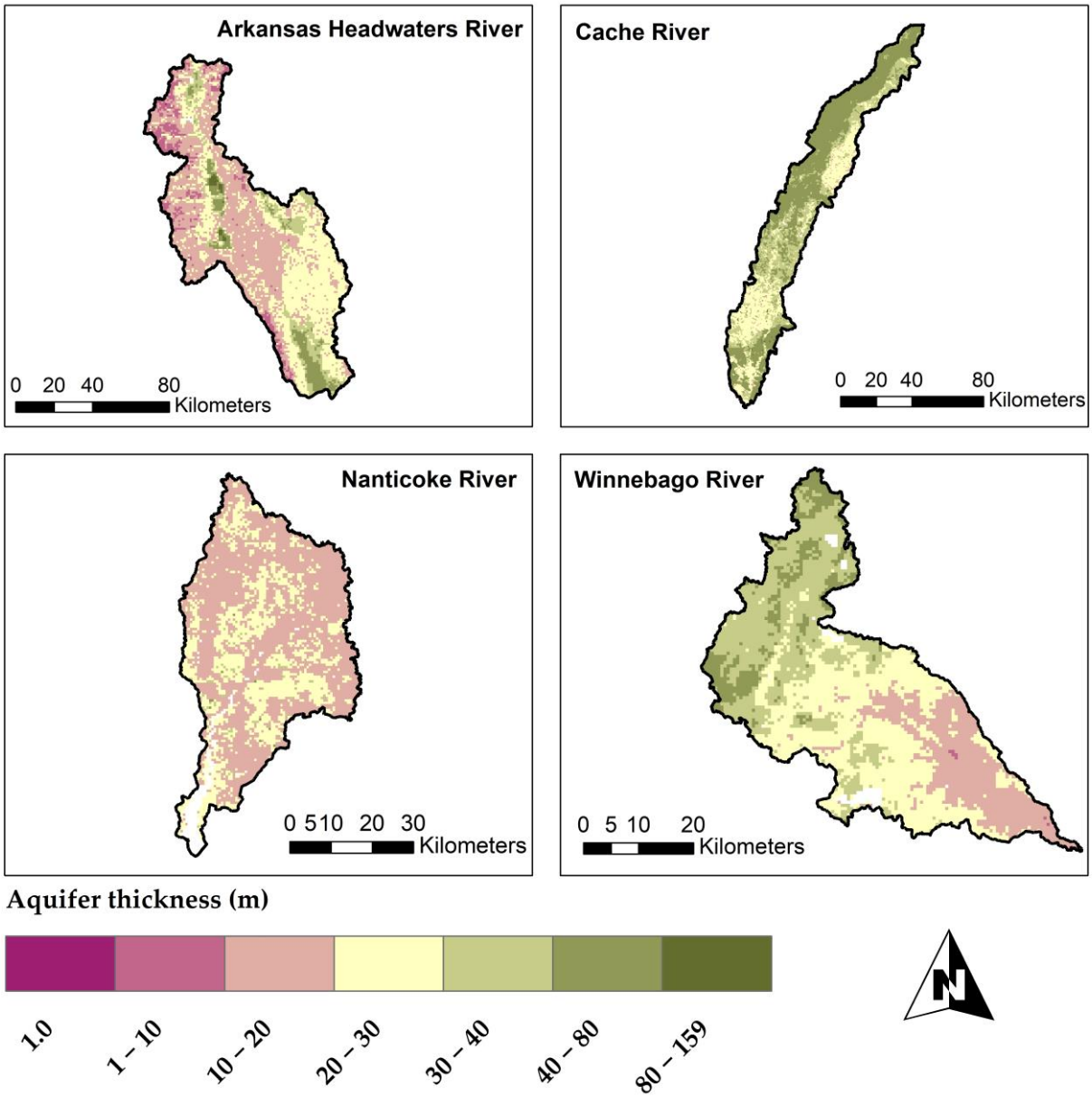


**Figure 5: Schematics representation aquifer thickness (m) maps for the four study watersheds of each grid cell.**

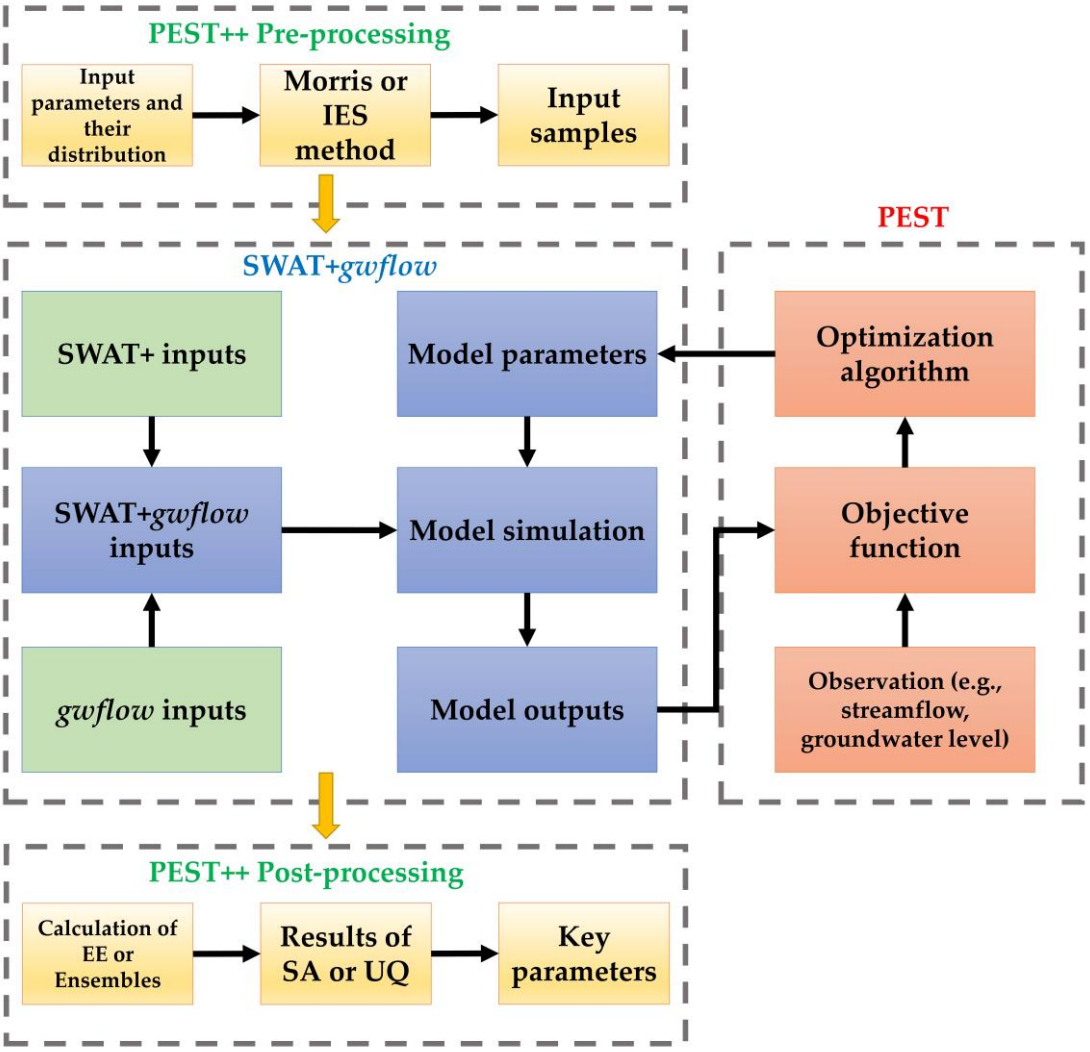


**Figure 6: Schematic of PEST automatic calibration, sensitivity analysis, and uncertainty analysis (iES) applied to the SWAT+*gwflow* models.**

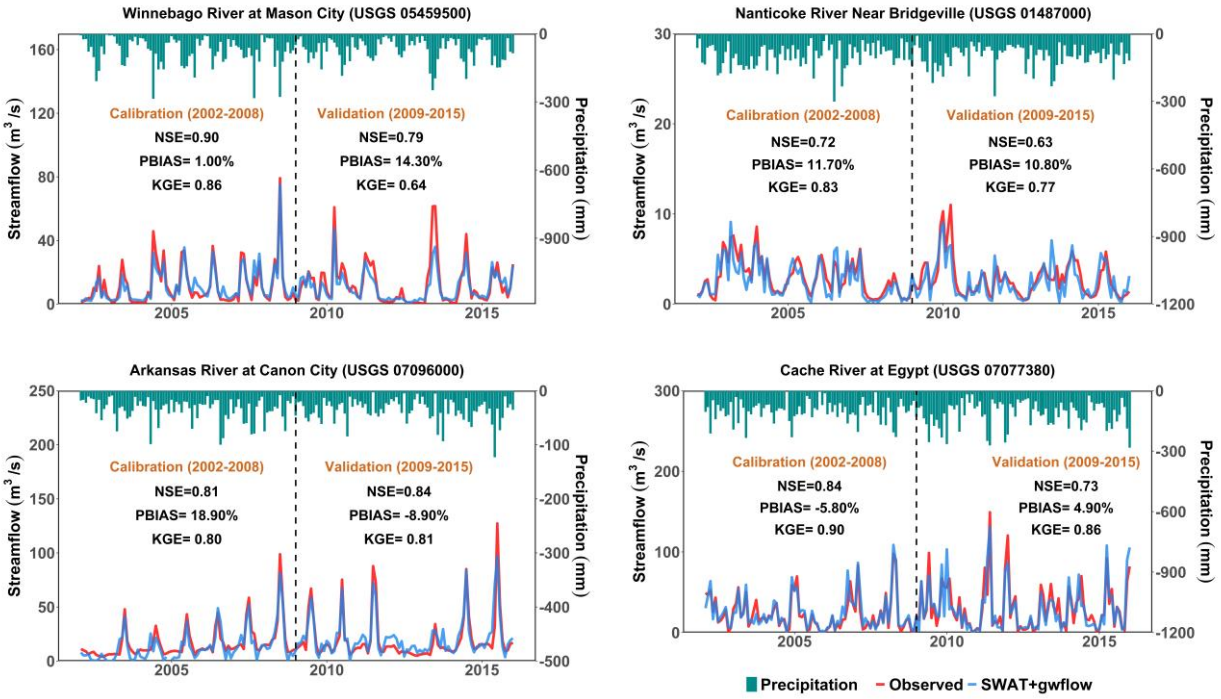


**Figure 7: Measured and simulated monthly streamflow for SWAT+*gwflow* models for four selected river gage stations within the four study watersheds. Statistical model performances (NSE, PBIAS, and KGE) are presented for each gage location.**

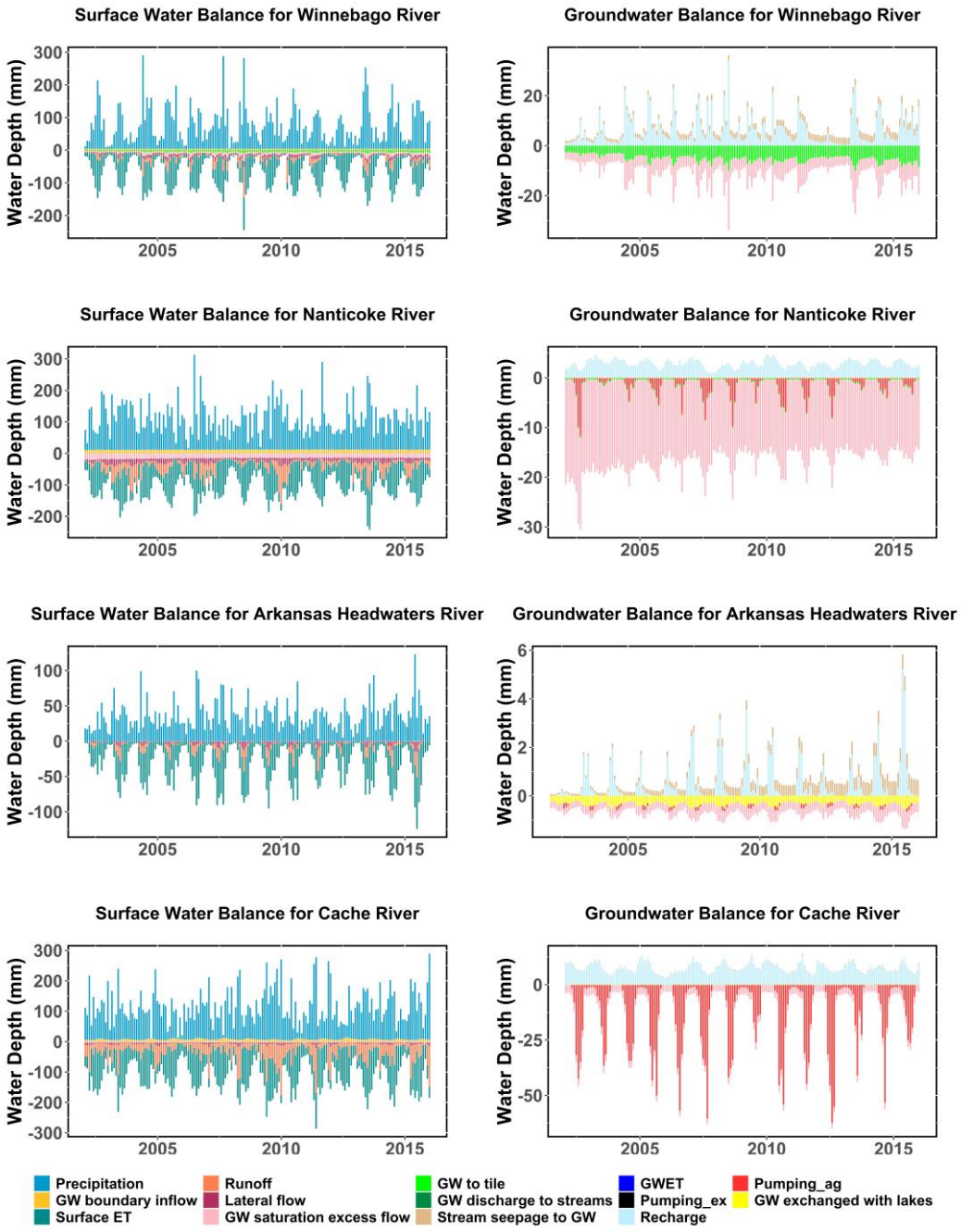


690 **Figure 8: Monthly surface water fluxes (mm) [left column], and groundwater fluxes (mm) [right column] for the simulation period of (2002–2015) for the four study watersheds.**

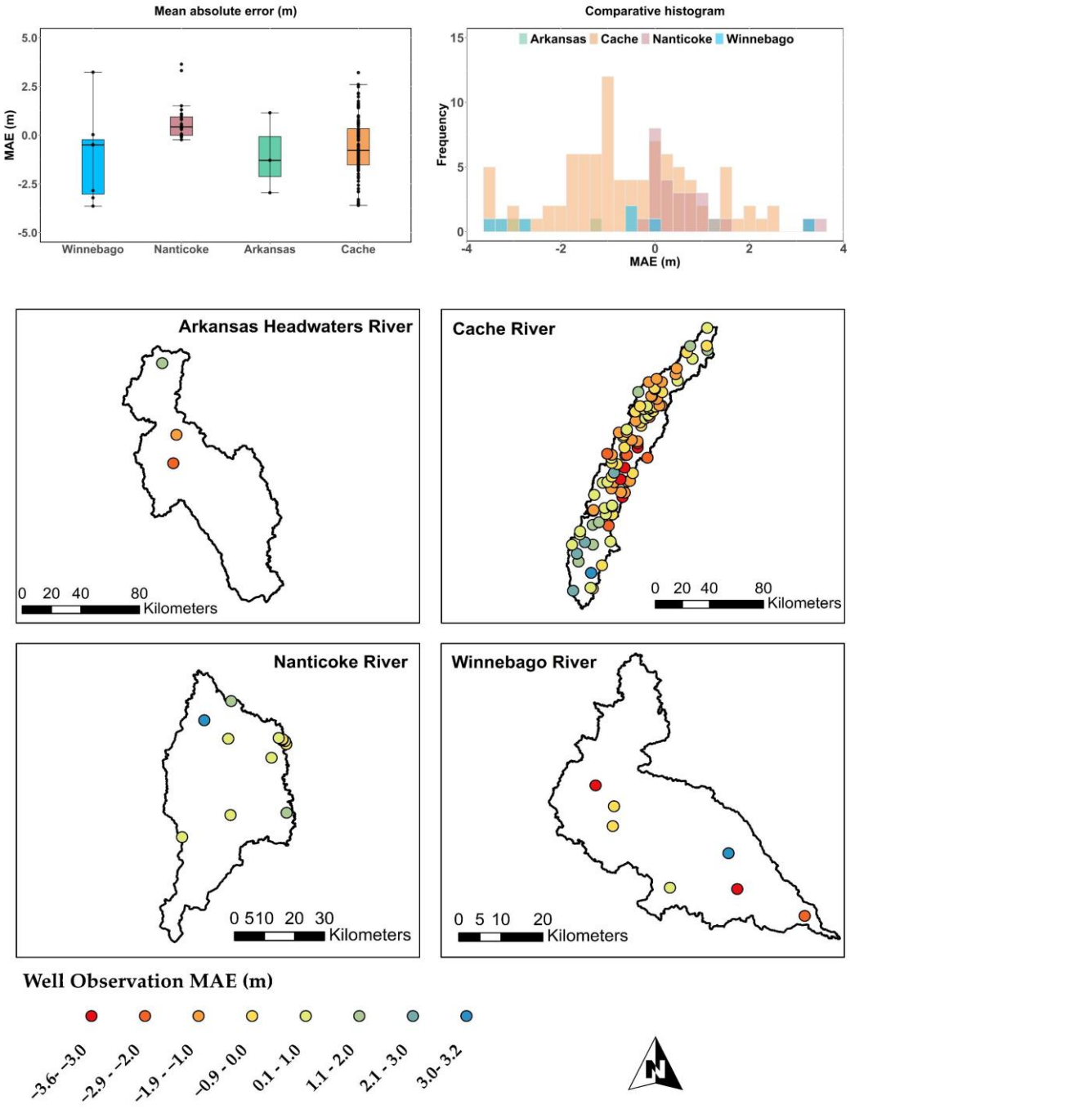


695 **Figure 9: Maps showing statistical model performance based on mean absolute error (MAE) (m) for groundwater level for the simulation period of (2000–2015) in the study watersheds.**

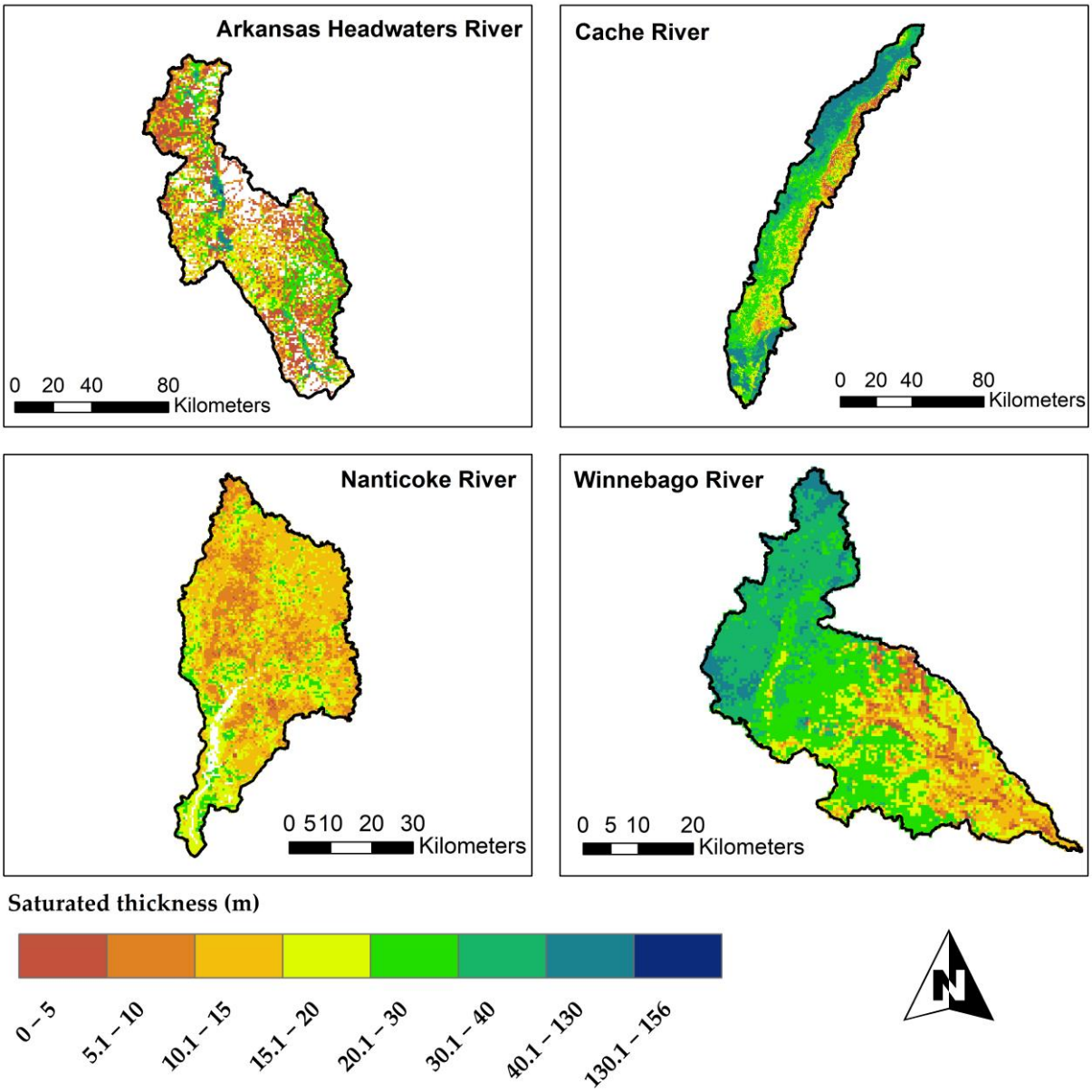


700

**Figure 10: Maps of saturated thickness (m) in the four study watersheds.**

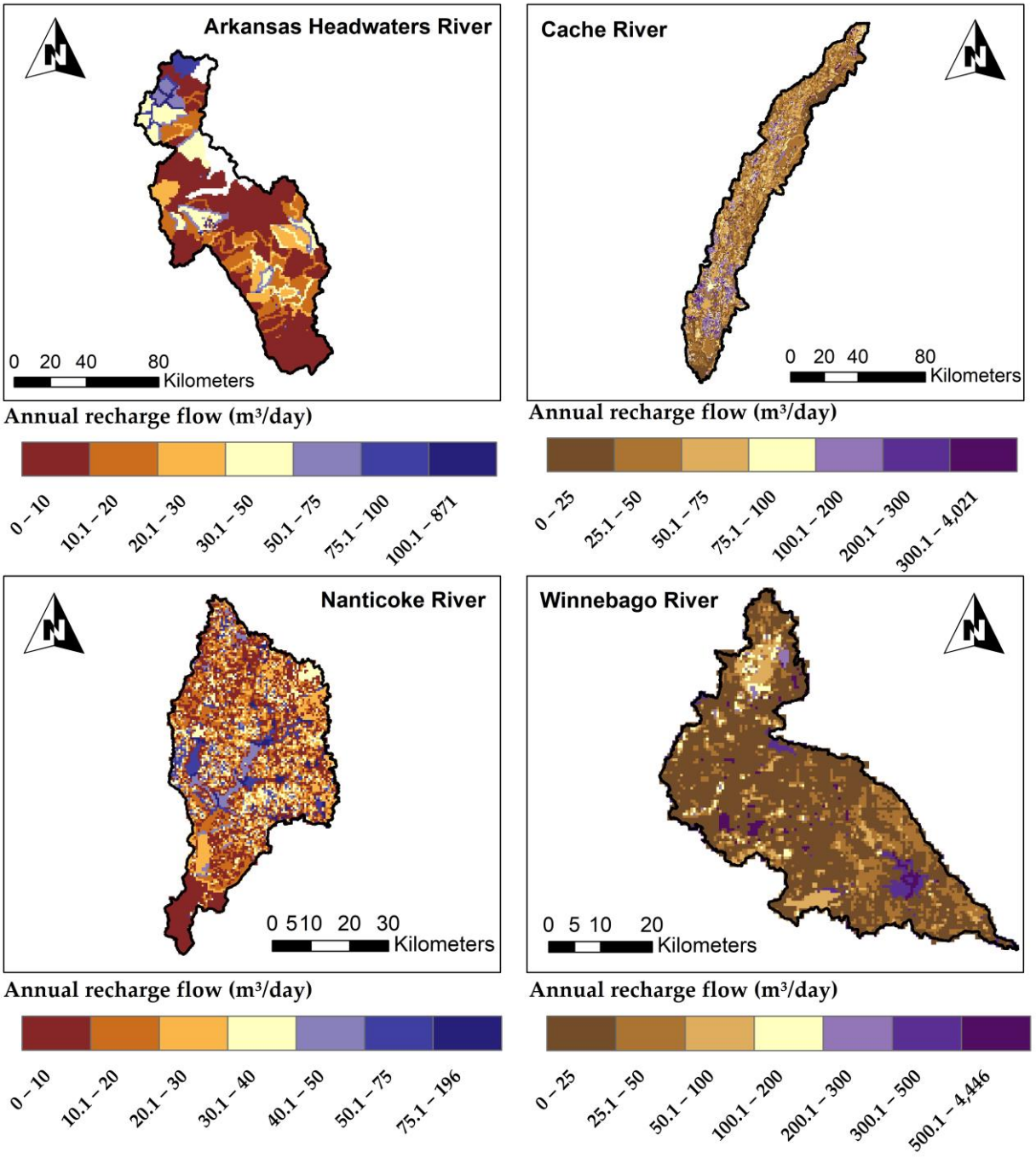


**Figure 11: Maps of average annual recharge flow ($m^3$/day) for the period of (2000–2015) for each of the study watersheds for each grid.**

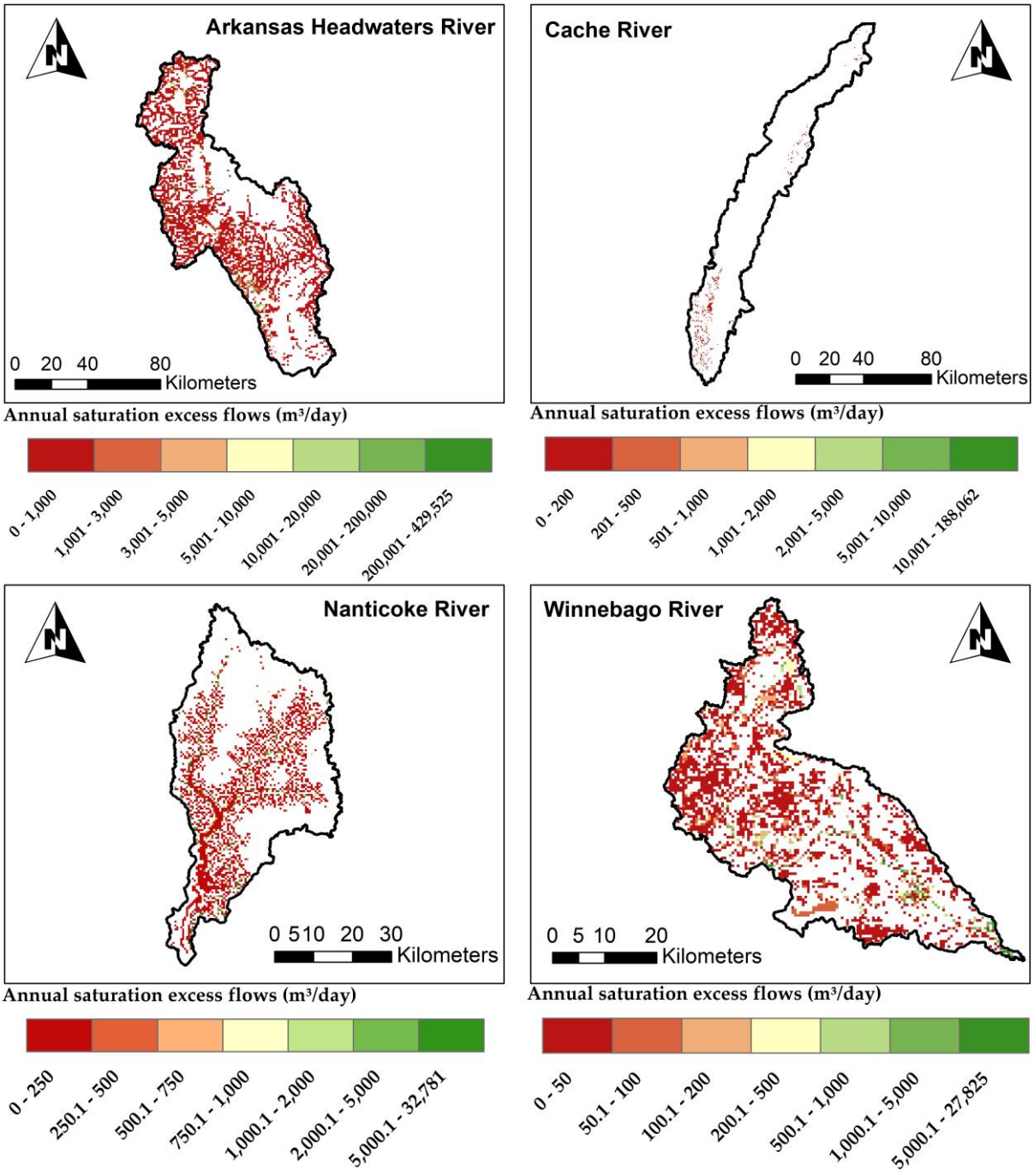


705

**Figure 12: Maps of average annual saturation excess flow ($m^3$/day) for the period of (2000–2015) in each of the four study watersheds for each grid.**

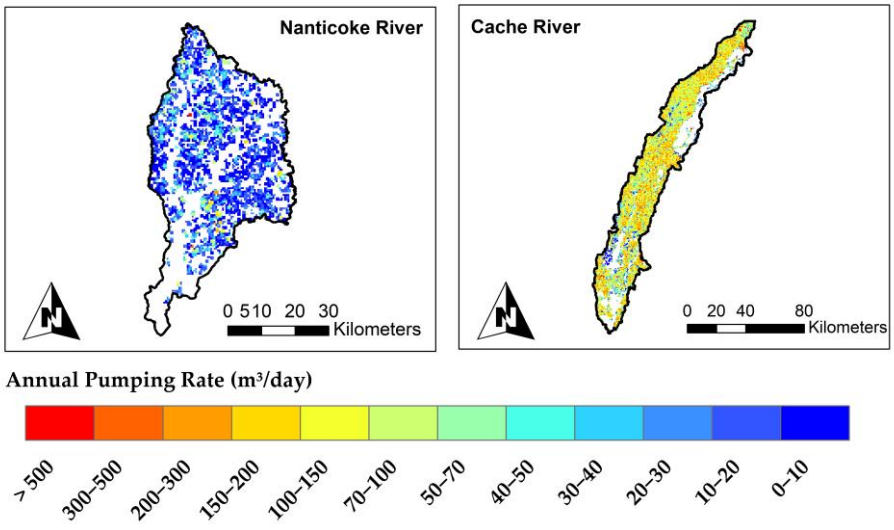


**Figure 13: Maps of average annual groundwater pumping for irrigation ($m^3$/day) in the Cache, and Nanticoke watersheds for each grid cell.**

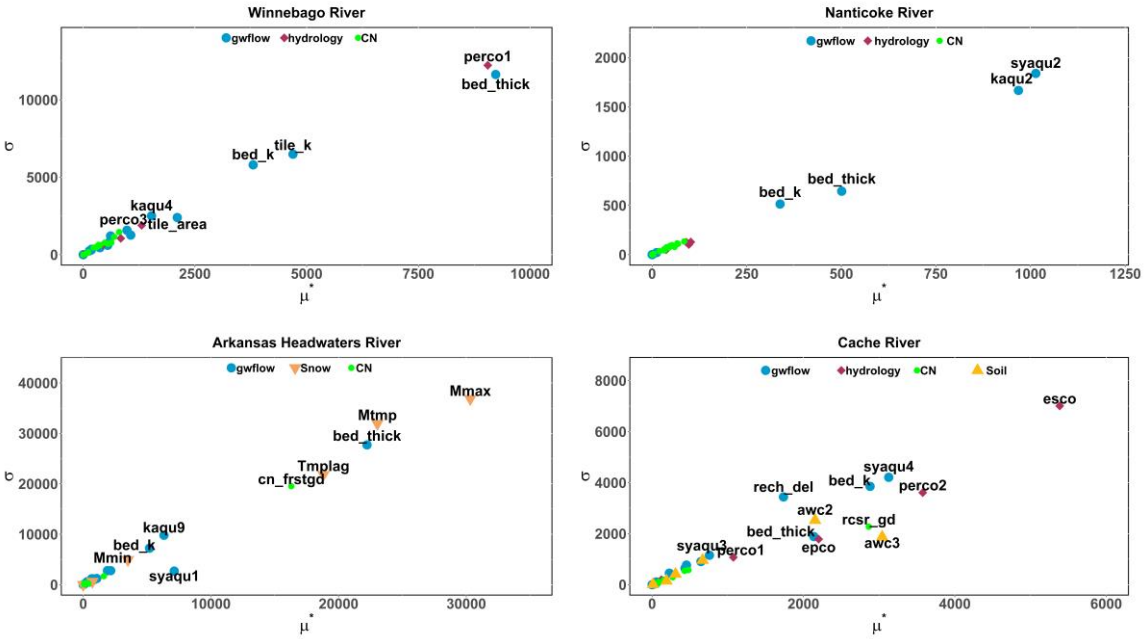


**Figure 14: Parameters sensitivity analysis based on the Morris screening method for minimizing streamflow. Only the most sensitive parameters are labelled. σ reveals the degree of nonlinearity or factor interaction, and μ* is the sensitivity measure. These sensitivity measures are based on elementary effects and are not related to the scale and magnitude of the input or output quantities; therefore, results show relative relation between parameters.**

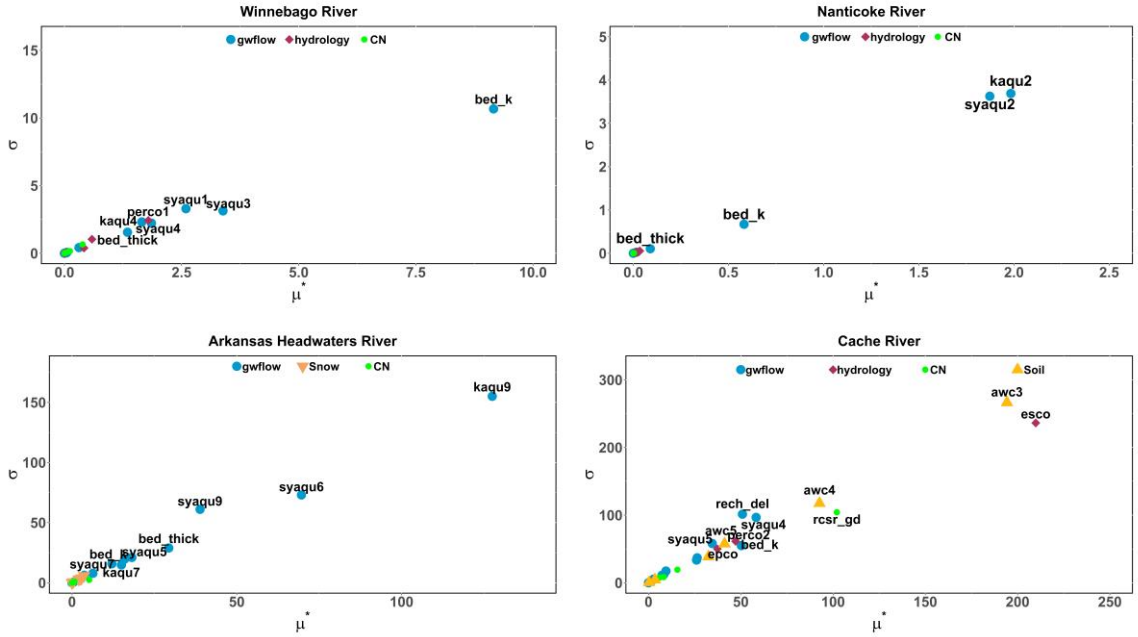


**Figure 15: Parameters sensitivity analysis based on the Morris screening method for minimizing groundwater level. Only the most sensitive parameters are labelled. σ reveals the degree of nonlinearity or factor interaction, and μ* is the sensitivity measure. These sensitivity measures are based on elementary effects and are not related to the scale and magnitude of the input or output quantities; therefore, results show relative relation between parameters.**

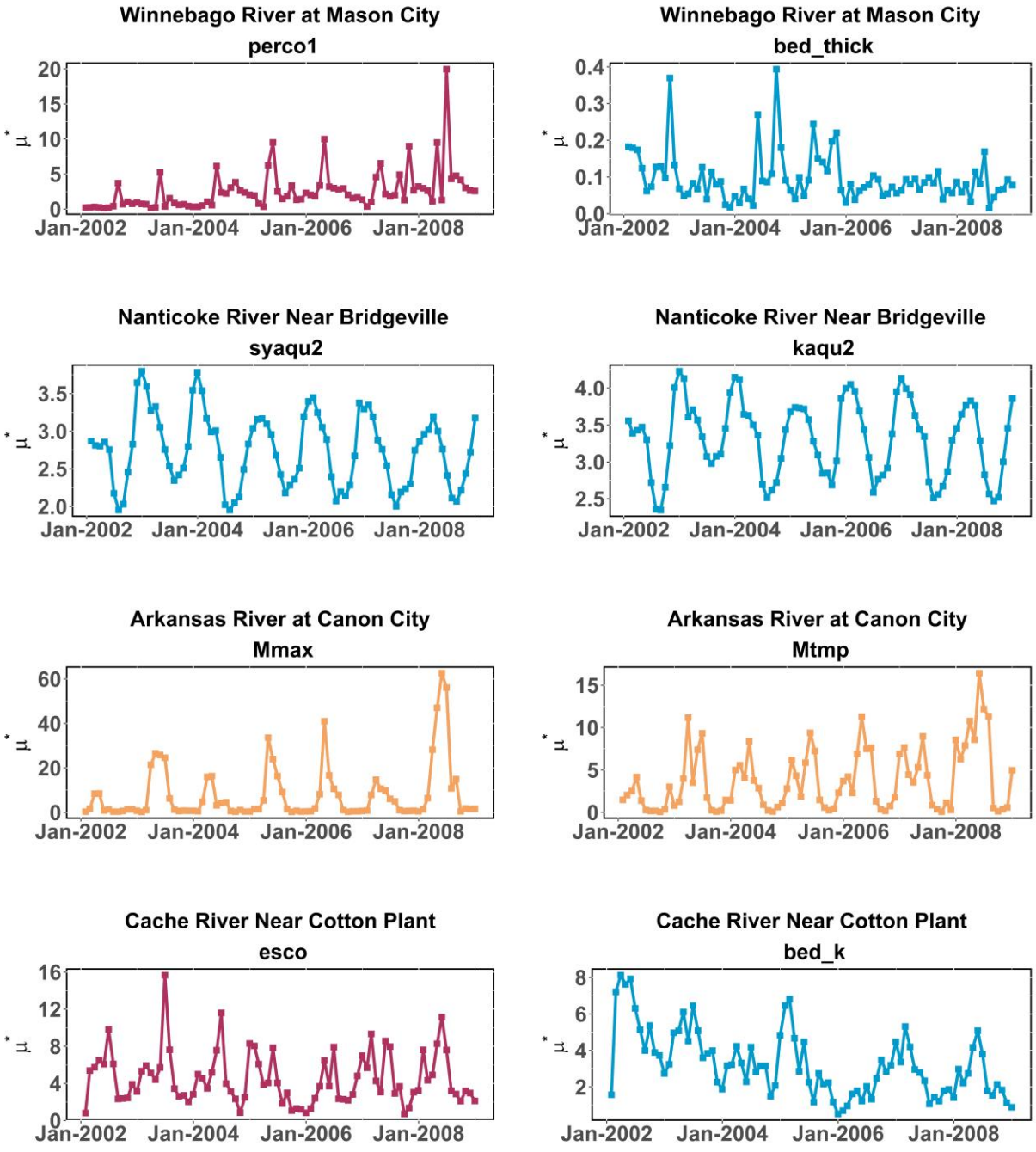


**Figure 16: Estimated sensitivity that changes with time for the streamflow for the key influential parameters of the four study watersheds. The blue lines represent *gwflow* parameters, maroon lines for hydrology parameters, and orange lines represent the snow parameters.**

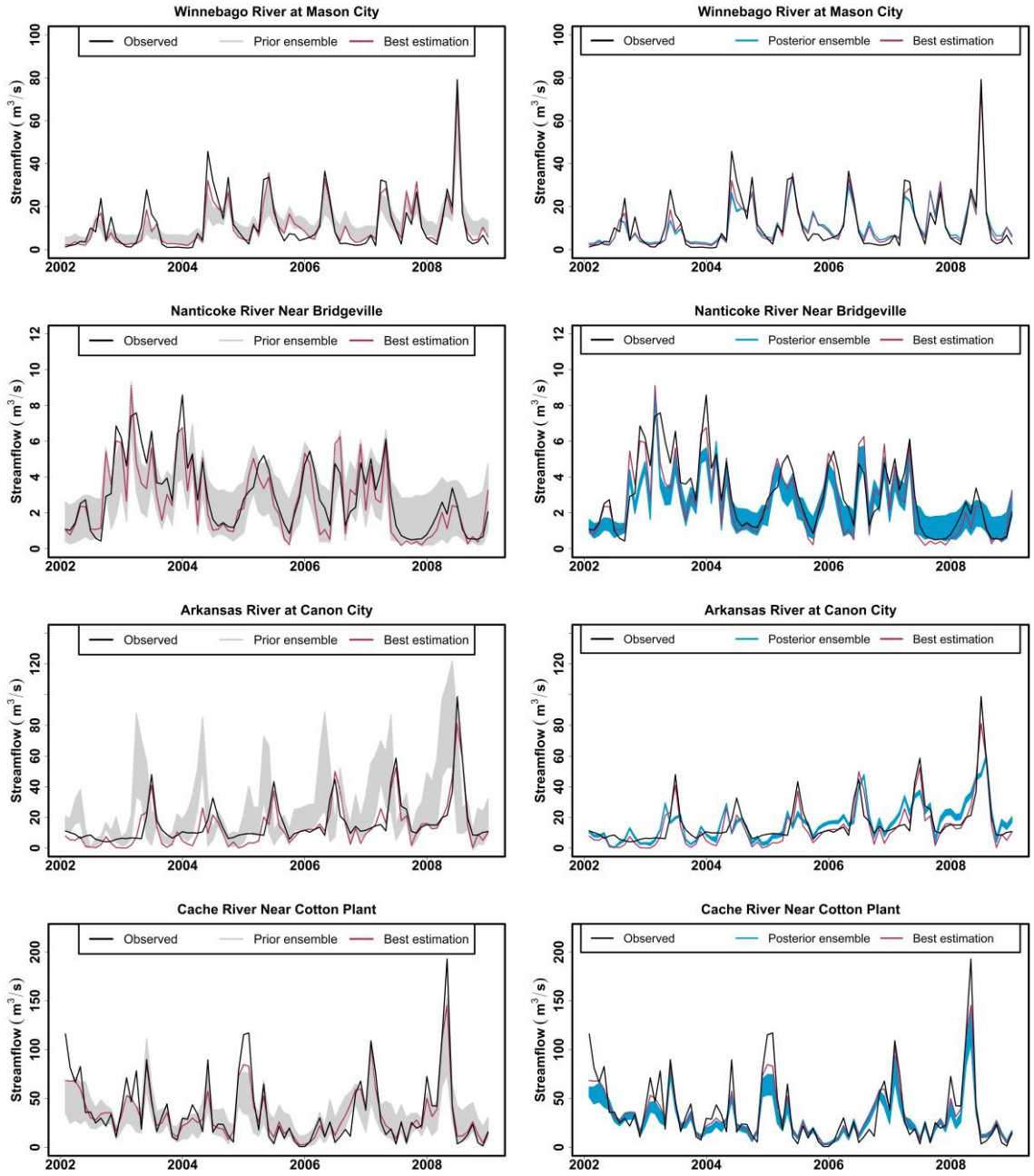


725

**Figure 17: Prior (left column) and posterior (right column) prediction uncertainty bounds for streamflow estimation for SWAT+*gwflow* for four study watersheds.**

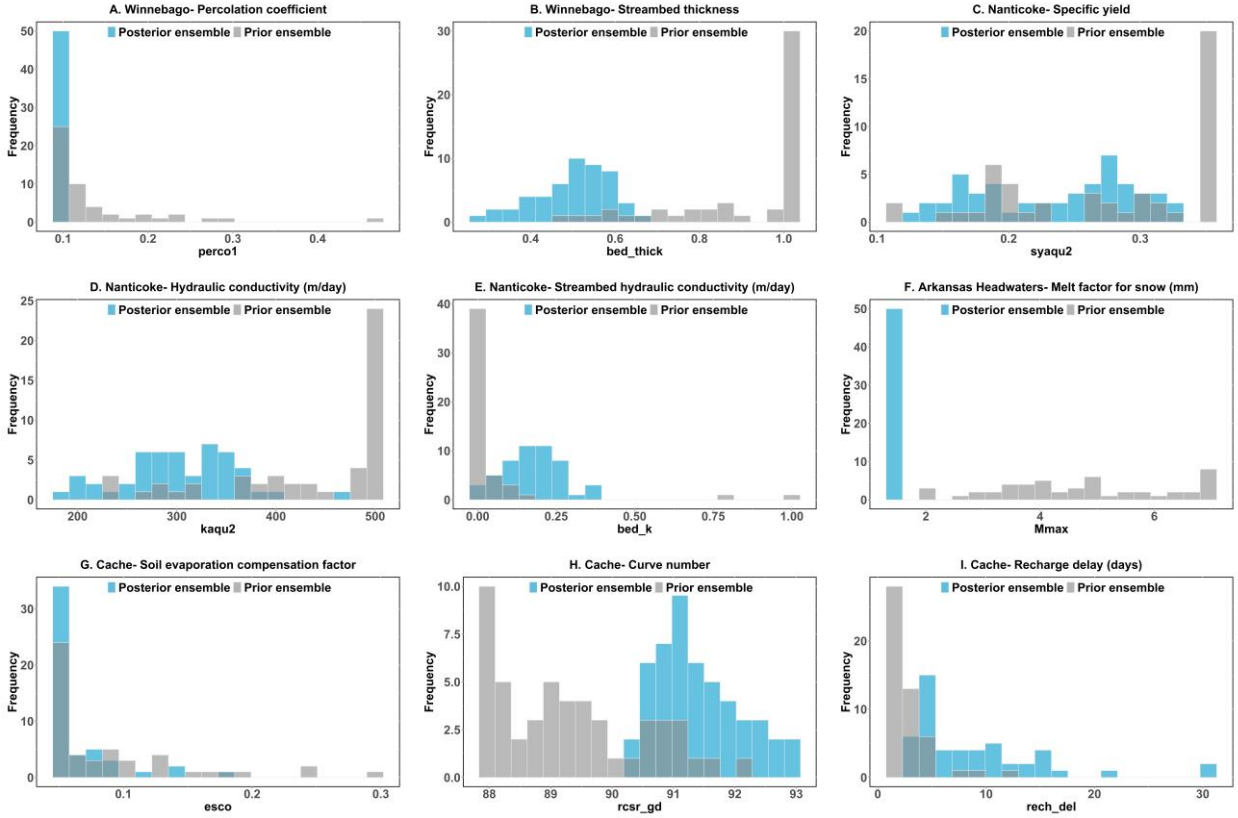


**Figure 18: Histogram for prior and posterior for significant parameters for four study watersheds.**

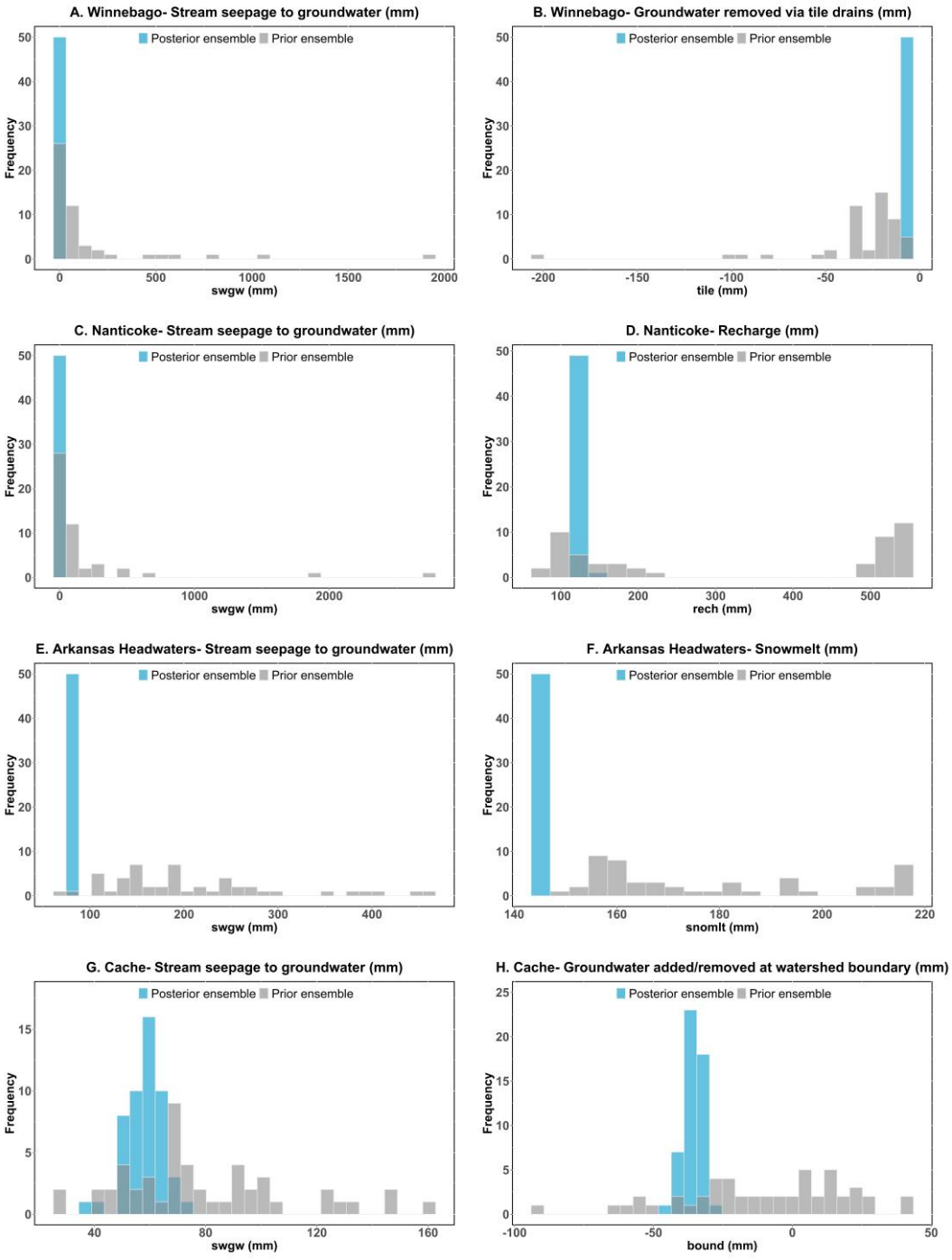


730

**Figure 19: Histogram for prior and posterior average annual water balance component (significant components) for four study watersheds.**

**Table 1.** Key features for the four study basins.

| | | | | | | *mm* | *km²* | *gwflow* grid | | |
|---|---|---|---|---|---|---|---|---|---|---|
| Watershed | State | HUC2 Region | HUC8 | # Channels | # HRU | Annual Precip. | Area | Rows | Cols | Cell size (m) |
| Winnebago | IA, MN | Upper Mississippi | 07080203 | 437 | 4358 | 880 | 1787 | 140 | 139 | 500 |
| Nanticoke | DE, MD | Mid Atlantic | 02080109 | 1069 | 5519 | 1180 | 2142 | 186 | 90 | 500 |
| Arkansas Headwaters | CO | Arkansas-White-Red | 11020001 | 2230 | 2986 | 425 | 7940 | 180 | 110 | 1000 |
| Cache | AR, MO | Lower Mississippi | 08020302 | 2941 | 17143 | 1287 | 5198 | 428 | 222 | 500 |

**Table 2.** Datasets utilized to create the *gwflow* inputs and the base SWAT+ models (Bailey et al., 2023)

| | Dataset | Resolution (m) | Source |
|---|---|---|---|
| **SWAT+ model** | Land use, Land cover | 30 | U.S. Geological Survey, National Land Cover Data |
| | Field boundaries | | Yan and Roy (2016) |
| | Topographic slope map | 10 | USGS National Elevation Dataset (Gesch et al., 2018) |
| | Weather | | Global historical climatology network; PRISM |
| | Soil boundaries and properties | 10 | Soil Survey Staff (2014) |
| | Stream segments (NHD+) | | Moore and Dewald (2016) |
| | Crop rotation | | USDA–NASS, CDL |
| | Lakes and reservoirs | | Moore and Dewald (2016) |
| | Water use | | Dieter et al. (2018) |
| | Discharge from facilities | | Skinner and Maupin (2019) |
| ***gwflow* module** | Groundwater head | Vector Points | Bailey and Alderfer (2022) |
| | Aquifer thickness | 250 | Shangguan et al. (2017) |
| | Tile drainage | 30 | Valayamkunnath et al. (2020) |
| | Geologic units | Vector Polygons | Horton et al. (2017) |

**Table 3.** Description of hydrological fluxes of **23** selected parameters for the SWAT+*gwflow* model.

| Parameters | Description of Parameter | Controlled Hydrologic Processes |
|---|---|---|
| **CN2** # | SCS runoff curve number | Surface runoff processes (cn) |
| **ESCO** # | Soil evaporation compensation factor | Potential and actual evapotranspiration processes (hydro) |
| **EPCO** # | Plant uptake compensation factor | |
| **rech_del** | Recharge delay (days) | Groundwater flow processes (*gwflow*) |
| **Kaqu** # | Aquifer hydraulic conductivity for a specific zone (m/day) for $i^{th}$ zone | |
| **Syaqu** # | Aquifer specific yield for a specific zone for $i^{th}$ zone | |
| **bed_k** | Streambed hydraulic conductivity (m/day) | |
| **bed_thick** | Streambed thickness (m) | |
| **bed_depth** | River depth (m) | |
| **tile_depth** | Depth of tiles below ground surface (m) | |
| **tile_area** | Area of groundwater inflow ($m^2$) to tile | |
| **tile_k** | Hydraulic conductivity of the drain perimeter (m/day) | |
| **Ftmp** | Snowfall temperature (°C) | Snow processes (sno) |
| **Snowd** | Minimum snow water content (mm $H_2O$) | |
| **Mmin** | Melt factor for snow on December 21 (mm $H_2O$/°C– day) | |
| **Mmax** | Melt factor for snow on June 21 (mm $H_2O$/°C– day) | |
| **Mtmp** | Snowmelt base temperature (°C) | |
| **Tmplag** | Snowpack temperature lag factor | |
| **COV50** | Fraction of COVMX | |
| **SOL_BD ()** | Moist bulk density ($g/cm^3$ or $Mg/m^3$) for $i^{th}$ layer | Soil water processes (sol) |
| **SOL_AWC ()** | Available water capacity of the soil layer (mm $H_2O$/mm soil) for $i^{th}$ layer | |
| **Perco** # | Percolation coefficient | |
| **SOL_K ()** | Saturated hydraulic conductivity (mm/h) for $i^{th}$ layer | |

**Table 4.** Selected parameters and ranges for the sensitivity and uncertainty analysis for the SWAT+*gwflow* model.

| Watershed | Parameter | No. of classes | Hydrologic process | Parameter range |
|---|---|---|---|---|
| **Nanticoke River** | rech_del | – | *gwflow* | 1 to 30 |
| | Kaqu # | 2 | *gwflow* | –80% to +100% (relative) |
| | Syaqu # | 2 | *gwflow* | 0.05 to 0.35 |
| | bed_k | – | *gwflow* | 0.0001 to 1 |
| | bed_thick | – | *gwflow* | 0.2 to 1 |
| | bed_depth | – | *gwflow* | –80% to +20% (relative) |
| | CN2 | 4 | cn | 0 to +30% (relative) |
| | esco | – | hydro | 0 to 1 |
| | epco | – | hydro | 0 to 1 |
| | perco | 2 | hydro | 0 to 1 |
| **Winnebago River** | rech_del | – | *gwflow* | 1 to 30 |
| | Kaqu # | 4 | *gwflow* | –90% to +100% (relative) |
| | Syaqu # | 4 | *gwflow* | 0.05 to 0.35 |
| | bed_k | – | *gwflow* | 0.0001 to 1 |
| | bed_thick | – | *gwflow* | 0.2 to 1 |
| | bed_depth | – | *gwflow* | –80% to +20% (relative) |
| | tile_depth | – | *gwflow* | 1 to 2 |
| | tile_area | – | *gwflow* | 10 to 100 |
| | tile_k | – | *gwflow* | 0.5 to 15 |
| | CN2 | 4 | cn | –12 to +12% (relative) |
| | esco | – | hydro | 0 to 1 |
| | epco | – | hydro | 0 to 1 |
| | perco | 3 | hydro | 0 to 1 |
| **Cache River** | rech_del | – | *gwflow* | 1 to 30 |
| | Kaqu # | 5 | *gwflow* | –80% to +100% (relative) |
| | Syaqu # | 5 | *gwflow* | 0.05 to 0.35 |
| | bed_k | – | *gwflow* | 0.0001 to 1 |
| | bed_thick | – | *gwflow* | 0.2 to 1 |
| | bed_depth | – | *gwflow* | –80% to +20% (relative) |
| | tile_depth | – | *gwflow* | 1 to 2 |
| | tile_area | – | *gwflow* | 10 to 60 |
| | tile_k | – | *gwflow* | 0.5 to 10 |
| | CN2 | 3 | cn | –7 to +33% (relative) |
| | esco | – | hydro | 0 to 1 |
| | epco | – | hydro | 0 to 1 |
| | perco | 4 | hydro | 0 to 1 |
| | awc | 6 | sol | 0 to 1 |
| **Arkansas Headwaters River** | Ftmp | – | sno | 0 to 5 |
| | Mtmp | – | sno | 0 to 5 |
| | Mmax | – | sno | 1.4 to 6.9 |
| | Mmin | – | sno | 1.4 to 6.9 |
| | Tmplag | – | sno | 0.01 to 1.01 |
| | Snowd | – | sno | 0.5 to 1 |
| | COV50 | – | sno | 0.1 to 1 |
| | CN2 | 2 | cn | –5 to +35% (relative) |
| | rech_del | – | *gwflow* | 1 to 30 |
| | Kaqu # | 9 | *gwflow* | –90% to +100% (relative) |
| | Syaqu # | 9 | *gwflow* | 0.05 to 0.35 |
| | bed_k | – | *gwflow* | 0.0001 to 1 |
| | bed_thick | – | *gwflow* | 0.2 to 1 |
| | bed_depth | – | *gwflow* | –80% to +20% (relative) |

**Table 5.** Monthly discharge statistical performance for the SWAT+*gwflow* simulation.

| River Basin | Station | Calibration | | | | Validation | | | |
|---|---|---|---|---|---|---|---|---|---|
| | | NSE | $R^2$ | PBIAS | KGE | NSE | $R^2$ | PBIAS | KGE |
| **Nanticoke River** | USGS 01488500 | 0.79 | 0.79 | –3.30 | 0.85 | 0.81 | 0.81 | –5.40 | 0.86 |
| | USGS 01487000 | 0.72 | 0.77 | 11.70 | 0.83 | 0.63 | 0.66 | 10.80 | 0.77 |
| **Winnebago River** | USGS 05459500 | 0.90 | 0.91 | 1.00 | 0.86 | 0.79 | 0.88 | 14.30 | 0.64 |
| **Cache River** | USGS 07077380 | 0.84 | 0.85 | –5.80 | 0.90 | 0.73 | 0.75 | 4.90 | 0.86 |
| | USGS 07077700 | 0.77 | 0.81 | 13.20 | 0.76 | **Not enough observations** | | | |
| | USGS 07077555 | 0.85 | 0.91 | 6.90 | 0.73 | 0.85 | 0.92 | 14.90 | 0.70 |
| **Arkansas Headwaters River** | USGS 07087050 | 0.91 | 0.92 | –6.90 | 0.91 | 0.94 | 0.95 | –8.60 | 0.91 |
| | USGS 07091200 | 0.91 | 0.93 | 3.80 | 0.90 | 0.96 | 0.96 | 0.60 | 0.96 |
| | USGS 07094500 | 0.73 | 0.84 | 23.10 | 0.75 | 0.84 | 0.85 | 7.30 | 0.84 |
| | USGS 07096000 | 0.81 | 0.85 | 18.90 | 0.80 | 0.84 | 0.85 | –8.90 | 0.81 |

**Table 6.** Model run times for simulation period of (2000–2015) for four study areas using standalone SWAT+ and holistic SWAT+*gwflow*.

| Watershed | Base SWAT+ (Minutes: seconds) | Holistic SWAT+*gwflow* (Minutes: seconds) |
|---|---|---|
| Winnebago River | 02: 37.10 | 07: 15.12 |
| Nanticoke River | 04: 30.00 | 11: 50.88 |
| Cache River | 12: 49.57 | 34: 43.75 |
| Arkansas Headwaters River | 05: 06.01 | 13: 23.92 |

**Table 7.** Mean annual hydrologic flow processes (mm) for 4 study watersheds with main fluxes fraction.

| | Flux (mm) | Winnebago | Nanticoke | Cache | Arkansas Headwaters |
|---|---|---|---|---|---|
| **Input** | Precipitation | 880 | 1180 | 1287 | 425 |
| | Boundary Inflow | 50 | 143 | 90 | – 2.40 |
| **Watershed Output** | Surface Runoff | 103 | 256 | 421 | 51 |
| | Sat Excess Flow | 75 | 183 | 37 | 4.6 |
| | Tile flow | 62 | 2.81 | 0.07 | 0.0 |
| | Stream seepage | 26 | 0.38 | 1.70 | 4.0 |
| | Soil Lateral Flow | 65 | 131 | 47 | 28 |
| | ET | 580 | 790 | 941 | 336 |
| **Internal Flows** | Recharge | 73 | 33 | 90 | 5.7 |
| | Pumping Irrigation | 0 | 15.5 | 141 | 0.42 |
| | GW-Lake Exchange | – 0.33 | – 0.70 | – 1.6 | – 4 |
| | Surface Water Irrigation | 0 | 1.00 | 43 | 0.14 |
| **Fractions** | Water Yield[a] | 279 | 573 | 504 | 80 |
| | Recharge Fraction[b] | 0.08 | 0.03 | 0.07 | 0.01 |
| | Yield Fraction[c] | 0.31 | 0.48 | 0.39 | 0.19 |
| | Baseflow Fraction[d] | 0.40 | 0.32 | 0.07 | 0.00 |
| | ET Fraction[e] | 0.65 | 0.66 | 0.72 | 0.79 |

a: Water Yield = Surface Runoff + Lateral Flow – Stream seepage + Saturation Excess Flow + Tile flow

795 b: Recharge / Precipitation

c: Water Yield / Precipitation

d: Net groundwater inflow to streams (Sat Excess Flow+ Tile flow–Stream Seepage) / Water Yield

e: ET / Precipitation

800